

This is the peer reviewed version of the following article:

Green's Function Formulation of Quantum Defect Embedding Theory / Sheng, Nan; Vorwerk, Christian; Govoni, Marco; Galli, Giulia. - In: JOURNAL OF CHEMICAL THEORY AND COMPUTATION. - ISSN 1549-9626. - 18:6(2022), pp. 3512-3522. [10.1021/acs.jctc.2c00240]

*Terms of use:*

The terms and conditions for the reuse of this version of the manuscript are specified in the publishing policy. For all terms of use and more information see the publisher's website.

12/01/2026 09:45

# Green’s function formulation of quantum defect embedding theory

Nan Sheng,<sup>†,§</sup> Christian Vorwerk,<sup>‡,§</sup> Marco Govoni,<sup>\*,‡,¶</sup> and Giulia Galli<sup>\*,‡,†,¶</sup>

<sup>†</sup>*Department of Chemistry, University of Chicago, Chicago, IL 60637, USA.*

<sup>‡</sup>*Pritzker School of Molecular Engineering, University of Chicago, Chicago, IL 60637, USA.*

<sup>¶</sup>*Materials Science Division and Center for Molecular Engineering, Argonne National Laboratory, Lemont, IL 60439, USA.*

<sup>§</sup>*These two authors contributed equally.*

E-mail: mgovoni@anl.gov; gagalli@uchicago.edu

## Abstract

We present a Green’s function formulation of the quantum defect embedding theory (QDET) where a double counting scheme is rigorously derived within the  $G_0W_0$  approximation. We then show the robustness of our methodology by applying the theory with the newly derived scheme to several defects in diamond. Additionally, we discuss a strategy to obtain converged results as a function of the size and composition of the active space. Our results show that QDET is a promising approach to investigate strongly correlated states of defects in solids.

## 1 Introduction

Electronic structure calculations of solids and molecules rely on the solution of approximate forms of the Schrödinger equation, for example using density functional theory,<sup>1–6</sup>

many-body perturbation theory,<sup>7-9</sup> or quantum chemistry methods<sup>10-12</sup> and, in some cases, quantum Monte Carlo.<sup>8</sup> Employing theoretical approximations is almost always necessary, as the solution of the electronic structure problem using the full many-body Hamiltonian of the system is still prohibitive, from a computational standpoint, for most molecules and solids, even in the case of the time independent Schrödinger equation.

Interestingly, there are important problems in condensed matter physics, materials science and chemistry for which a specific region of interest may be identified, a so-called active region, surrounded by a host medium, and for which the electronic structure problem can be solved at a high level of theory, for example, by exact diagonalization. An active region may be associated, for instance, to point defects in materials, active site of catalysts or nanoparticles embedded in soft or hard matrices. All of these problems may then be addressed using embedding theories<sup>13-15</sup> which separate the electronic structure problem of the active region from that of the host environment. Each part of the system is described at the quantum-mechanical level,<sup>13</sup> at variance with quantum embedding models, e.g. QM/MM, where only the active space or region is described with quantum-mechanical methods, while the environment is treated classically.<sup>16,17</sup>

Several embedding techniques have been proposed in the literature in recent years, which may be classified by the level of theory chosen to describe the different portions of the system. Density-based theories encompass density-functional-theory embedding in-density-functional-theory (DFT-in-DFT) and wavefunction embedding in-DFT (WF-in-DFT).<sup>18-20</sup> In these schemes the environment is described within DFT and the active region with a level of DFT higher than that adopted for the environment or with quantum-chemical, wavefunction based methods. Density-matrix embedding theory (DMET)<sup>21-27</sup> employs instead the density matrix of the system to define an embedding protocol. Finally, Green's ( $G$ ) function-based quantum embedding methods include the self-energy embedding<sup>28-30</sup>, dynamical mean field (DMFT)<sup>31-35</sup> and the quantum defect embedding theories (QDET).<sup>15,36,37</sup>

QDET is a theory we have recently proposed for the calculation of defect properties in

solids, with the goal of computing strongly correlated states which may not be accurately obtained using mean field theories, such as DFT, when using large supercells. However, the applicability of the theory is not restricted to defects in solids and QDET may be used to study, in general, a small guest region embedded in a large host condensed system. Similar to all Green’s function based methods, in QDET the active space is defined by a set of single-particle electronic states. The set includes the states localized in proximity of the defect or impurity and, in some cases, contains additional single-particle orbitals.

The embedding protocol used in QDET leads to a delicate problem that many embedding theories have in common, at least conceptually: the presence of “double counting” terms in the effective Hamiltonian of the active regions. These are terms that are computed both at the level of theory chosen for the active region and at the lower level chosen for the environment. Hence corrections (often called double counting corrections) are required to restore the accuracy of the effective Hamiltonian.

In the original formulation of QDET presented in Ref. 37, we adopted an approximate double counting correction based on Hartree-Fock theory. Here we present a more rigorous derivation of QDET based on Green’s functions and we derive a double counting correction that is exact within the  $G_0W_0$  approximation and when retardation effects are neglected. We call this correction EDC@ $G_0W_0$  (*exact* double counting at  $G_0W_0$  level of theory). We then apply QDET with the EDC@ $G_0W_0$  scheme to several spin defects in solids and we present a strategy to systematically converge the results as a function of the composition and size of the active space. Finally we show that using the EDC@ $G_0W_0$ , we obtain results for the electronic structure of spin defects consistent with experiments and in good agreement with results obtained with other embedding theories.<sup>38</sup>

The rest of the paper is organized as follows. Section 2 presents the formulation of QDET and Section 3 its implementation. Our results are presented in Section 4 and conclusions in Section 5.

## 2 Formulation of quantum defect embedding theory (QDET)

In Ref. 36,37 we introduced the Quantum Defect Embedding Theory (QDET), an embedding scheme that describes a condensed system where the electronic excitations of interest occur within a small subspace (denoted as the active space  $A$ ) of the full Hilbert space of the system. The formulation is based on the description of the system using periodic DFT and assumes that the interaction between active regions belonging to periodic replicas may be neglected (*i.e* the dilute limit). We summarize below the original formulation of the QDET method, including the approximate double counting scheme used in Ref. 36,37. We then present a Green's function formulation of QDET which enables the definition of an improved correction to the double counting scheme originally adopted, which is exact within the  $G_0W_0$  approximation.

In QDET an active space is defined as the space spanned by an orthogonal set of functions  $\{\zeta_i\}$ , for instance, selected eigenstates of the Kohn-Sham (KS) Hamiltonian describing a solid, or localized functions, *e.g.*, Wannier orbitals constructed from Kohn-Sham eigenstates through a unitary transformation. Within the Born-Oppenheimer and nonrelativistic approximations, the many-body effective Hamiltonian of a system of interacting electrons within a given active space takes the following form:

$$H^{\text{eff}} = \sum_{ij}^A t_{ij}^{\text{eff}} a_i^\dagger a_j + \frac{1}{2} \sum_{ijkl}^A v_{ijkl}^{\text{eff}} a_i^\dagger a_j^\dagger a_l a_k, \quad (1)$$

where  $t^{\text{eff}}$  and  $v^{\text{eff}}$  are one- and two-body terms that include the influence of the environment on the chosen active space. In QDET, these terms are determined by first carrying out a mean-field calculation of the full solid using, *e.g.*, DFT. Once the KS eigenstates and eigenvalues of the full system are obtained, the two-body terms  $v^{\text{eff}}$  are computed as the

matrix elements of the partially screened static Coulomb potential  $W_0^R$ , *i.e.*,

$$v_{ijkl}^{\text{eff}} = [W_0^R]_{ijkl} := \int d\mathbf{x} d\mathbf{x}' \zeta_i(\mathbf{x}) \zeta_k(\mathbf{x}) W_0^R(\mathbf{x}, \mathbf{x}'; \omega = 0) \zeta_j(\mathbf{x}') \zeta_l(\mathbf{x}'). \quad (2)$$

The term  $W_0^R$  in Eq. 2 is obtained by screening the bare Coulomb potential  $v$  with the reduced polarizability  $P_0^R$ , defined by the following equation:

$$W_0^R = v + v P_0^R W_0^R. \quad (3)$$

The reduced polarizability may be obtained by subtracting from the total irreducible polarizability of the periodic system the contribution from the active space, namely  $P_0^R = P_0 - P_0^A$ . Within the Random-Phase Approximation (RPA), the active space polarizability  $P_0^A$  is given by

$$P_0^A(\mathbf{x}_1, \mathbf{x}_2; \omega) = \sum_i^{\text{occ}} \sum_j^{\text{unocc}} (f^A \psi_i^{\text{KS}})(\mathbf{x}_1) (f^A \psi_j^{\text{KS}})(\mathbf{x}_1) (f^A \psi_j^{\text{KS}})(\mathbf{x}_2) (f^A \psi_i^{\text{KS}})(\mathbf{x}_2) \times \left( \frac{1}{\omega - (\epsilon_j^{\text{KS}} - \epsilon_i^{\text{KS}}) + i\eta} + \frac{1}{\omega + (\epsilon_j^{\text{KS}} - \epsilon_i^{\text{KS}}) - i\eta} \right), \quad (4)$$

where  $\psi_i^{\text{KS}}$  and  $\epsilon_i^{\text{KS}}$  are the Kohn-Sham eigenfunctions and -values, respectively and “occ” and “unocc” denote sums over occupied and empty states, respectively. Here, we have introduced the projector  $f^A = \sum_i^A |\zeta_i\rangle \langle \zeta_i|$  on the active space. An expression of the total irreducible polarizability may be obtained by omitting the projectors  $f^A$  on the RHS of Eq. 4. In Refs. 36,37 we proposed an efficient implementation of Eq. 4 that does not require any explicit summation over unoccupied states, thus enabling the application of QDET to large systems.

The definition of  $v^{\text{eff}}$  given above includes contributions to the Hartree and exchange correlation energies that are also included in the DFT calculations for the whole solid, *i.e.*, it contains so-called double counting (dc) terms. The latter are subtracted (that is corrections

to double counting contributions are applied) when defining the one-body terms  $t^{\text{eff}}$ ,

$$t_{ij}^{\text{eff}} = H_{ij}^{\text{KS}} - t_{ij}^{\text{dc}}, \quad (5)$$

where  $H^{\text{KS}}$  is the Kohn-Sham Hamiltonian.

## 2.1 QDET based on density functional theory

In previous applications of QDET, the double counting term  $t^{\text{dc}}$  was approximated, since within a DFT formulation of the theory, one cannot define an explicit expression for the exchange and correlation potential for a subset of electronic states. Therefore, an approximate form of  $t^{\text{dc}}$  inspired by Hartree-Fock was used, given by:

$$t_{ij}^{\text{dc}} \approx \sum_{kl}^A \left( [W_0^R(\omega = 0)]_{ikjl} - [W_0^R(\omega = 0)]_{ijkl} \right) \rho_{kl}^A, \quad (6)$$

where the reduced density matrix of the active space  $A$  is given by  $\rho_{ij}^A = \sum_k^{\text{occ}} \langle \zeta_i | \psi_k \rangle \langle \psi_k | \zeta_j \rangle$ .

Once the terms in the Hamiltonian of Eq. 1 are defined, the electronic structure of the correlated states in the active space  $A$  is obtained from an exact diagonalization procedure, using the full configuration interaction (FCI) method.

We note that within Hartree-Fock theory, the expression of  $t^{\text{dc}}$ , where  $v$  replaces  $W_0^R$  on the RHS of Eq. 6, is exact; however Eq. 6 turns out to be an approximate expression when used within DFT. While QDET with an approximate double counting scheme has been successfully applied to a range of defects in diamond and SiC, the influence of the approximation used for  $t^{\text{dc}}$  deserves further scrutiny. Most importantly, a formulation without double counting approximations is desirable.

In the next section, we present a Green's function formulation of QDET and we derive an analytical expression for  $t^{\text{eff}}$  that in turns leads to an expression for the double counting term  $t^{\text{dc}}$  which is exact within the  $G_0W_0$  approximation.

## 2.2 Green's function formulation of QDET

Instead of starting by a DFT formulation, we describe the interacting electrons in a solid by defining the one-body Green's function  $G$  and the screened Coulomb potential  $W$ . The reason to introduce a Green's function description stems from the fact that the self-energy  $\Sigma$  and its irreducible polarizability  $P$  can be written as sums of contributions from different portions of the entire system. The basic equations relating  $G$ ,  $W$ ,  $\Sigma$  and  $P$  are:

$$G^{-1} = g^{-1} - \Sigma \quad (7)$$

$$W^{-1} = v^{-1} - P, \quad (8)$$

where  $v$  is the bare Coulomb potential; the bare Green's function  $g = (\omega - h)^{-1}$  with  $h = -\frac{1}{2}\nabla^2 + v_{\text{ion}}$ , where  $v_{\text{ion}}$  is the electrostatic potential of the nuclei.

We chose two different levels of theory to describe different portions of the system, namely we describe the active space with a so-called higher level theory (high) than that applied to the whole system (low). We write the self-energy and polarizability of the whole system as:

$$\Sigma = \Sigma^{\text{low}} + (\Sigma^{\text{high}} - \Sigma^{\text{dc}})_A \quad (9)$$

$$P = P^{\text{low}} + (P^{\text{high}} - P^{\text{dc}})_A. \quad (10)$$

Here, we introduced the double counting terms  $\Sigma^{\text{dc}}$  and  $P^{\text{dc}}$  that correct for the contributions to the self-energy and polarizability of the active space  $A$ , which are included both in the high- and low-level descriptions of  $A$ . The terms with subscript  $A$  in Eqs. 9 and 10 are defined in the subspace  $A$ . Inserting Eqs. 9 and 10 into Eq. 7 and 8, respectively, leads to

$$G^{-1} = [G^R]^{-1} - \Sigma_A^{\text{high}} \quad (11)$$

$$W^{-1} = [W^R]^{-1} - P_A^{\text{high}}, \quad (12)$$



where we have defined the renormalized Green's function  $G^R$  and partially screened potential  $W^R$  as:

$$[G^R]^{-1} = g^{-1} - \Sigma^{\text{low}} + \Sigma_A^{\text{dc}} \quad (13)$$

$$[W^R]^{-1} = v^{-1} - P^{\text{low}} + P_A^{\text{dc}}. \quad (14)$$

Comparing Eq. 11 and 12 with Eq. 7 and 8, we find that the problem of determining  $G$  and  $W$  for the total system  $A + E$  has been simplified: only a solution with the high-level method within  $A$  is necessary to obtain  $G$  and  $W$ . To obtain such solution, the bare Green's function  $g$  and bare Coulomb potential  $v$  should be replaced by their renormalized counterparts  $G^R$  and  $W^R$ , respectively. We now turn to derive expressions for  $\Sigma^{\text{low}}$  and  $P^{\text{low}}$ , and  $\Sigma^{\text{high}}$  and  $P^{\text{high}}$ , which will then allow for the definition of all terms entering the effective Hamiltonian of the active space.

### 2.2.1 Effective Hamiltonian

Under the assumption that retardation effects may be neglected, *i.e.*, assuming that one- and two-body interactions within  $A$  are instantaneous, we can derive a simple equation relating  $G^R$  and  $W^R$  and the parameters of the effective Hamiltonian in Eq. 1. In the absence of retardation effects, the effective Green's function  $G^R$  is given by the Lehmann representation and we have:

$$G^R(\omega) \approx [\omega - t^{\text{eff}}]^{-1}. \quad (15)$$

Note that the validity of this equation rests on the assumption that the non-diagonal terms of the self-energy coupling the active space and the environment are negligible, *i.e.*  $(\Sigma^{\text{low}})_{AE} = 0$ . Eq. 15 defines the one-body terms  $t^{\text{eff}}$  of Eq. 1. To derive the two-body terms, we neglect the frequency dependence of the screened Coulomb interaction and write:

$$v_{ijkl}^{\text{eff}} \approx \int d\mathbf{x} d\mathbf{x}' \zeta_i(\mathbf{x}) \zeta_k(\mathbf{x}) W^R(\mathbf{x}, \mathbf{x}', \omega = 0) \zeta_j(\mathbf{x}') \zeta_l(\mathbf{x}'). \quad (16)$$

We note that the static approximation of the screened Coulomb interaction is commonly employed to calculate neutral excitations in solids and molecules within many-body perturbation theory (MBPT),<sup>8</sup> and it has been shown to yield neutral excitations in a wide range of materials with excellent accuracy. In order to obtain the expressions of  $t^{\text{eff}}$  and  $v^{\text{eff}}$  for which an analytic expression of  $t^{\text{dc}}$  can be derived, we turn to the  $G_0W_0$  approximation, which we use as low level of theory for the entire system. Such a choice of low-level theory enables the separation of the self-energy as required by Eq. 9.

### 2.2.2 $G_0W_0$ approximation as low-level theory

We use the  $G_0W_0$  approximation and write  $\Sigma^{\text{low}} = \Sigma^{G_0W_0}$  with

$$\Sigma^{G_0W_0} = V_{\text{H}} + \Sigma_{\text{xc}} = v\rho + iG_0W_0. \quad (17)$$

(See SI for additional details). We evaluate the Green's function  $G_0$  using the KS Hamiltonian, *i.e.*,

$$G_0(\omega) = (\omega - H^{\text{KS}})^{-1}. \quad (18)$$

The screened Coulomb potential is obtained as  $W_0^{-1} = v^{-1} - P_0$ , with

$$P_0 = -iG_0G_0. \quad (19)$$

### 2.2.3 Double counting correction

To derive the double counting terms  $\Sigma^{\text{dc}}$  and  $P^{\text{dc}}$ , we require that the chain rule be satisfied, *i.e.*, that when using the low-level of theory to describe both the total system ( $A+E$ ) and the active space ( $A$ ), the total self-energy and the total polarizability on the LHS of Eq. 9 and 10 are the same as  $\Sigma^{\text{low}}$  and  $P^{\text{low}}$ , respectively. This requirement implies that  $\Sigma^{\text{dc}}$  and  $P^{\text{dc}}$  coincide with the self-energy and the polarizability derived from the effective Hamiltonian expressed at the low-level of theory. Within the  $G_0W_0$  approximation, this requirement leads

to the following expressions

$$\Sigma^{\text{dc}} = \Sigma_{G_0 W_0}^{\text{eff}} \quad (20)$$

$$P^{\text{dc}} = P_0^{\text{eff}}. \quad (21)$$

Here the superscript ‘eff’ indicates that the self-energy and polarizabilities are computed for  $H^{\text{eff}}$ ; these quantities are different from the corresponding ones evaluated for  $H$  projected onto  $A$ . The double counting contribution to the polarizability,  $P^{\text{dc}}$ , is obtained with Eq. 19 after restricting the Green’s function to  $A$ , *i.e.*,

$$P^{\text{dc}} = P_0^A = -iG_0^A G_0^A, \quad (22)$$

with  $G_0^A = f^A G_0 f^A$ . Eq. 14 and 22 allow us to determine the partially screened Coulomb potential  $W_0^R$  as

$$[W_0^R]^{-1} = v^{-1} - (G_0^A G_0^R + G_0^R G_0^A + G_0^R G_0^R) = v^{-1} - P_0^R, \quad (23)$$

where we have defined the reduced Kohn-Sham Green’s function  $G_0^R = G_0 - G_0^A$ . The matrix elements of  $W_0^R$  thus enter the definition of the two-body terms of the effective Hamiltonian. Hence we have shown that by framing QDET within the context of Green’s embedding theories we recover Eq. 3.

Similar to the derivation of  $P^{\text{dc}}$ , the double counting contribution to the self-energy,  $\Sigma^{\text{dc}}$ , is given by the  $G_0 W_0$  self-energy associated to  $H^{\text{eff}}$ , *i.e.*,  $\Sigma_{G_0 W_0}^{\text{eff}} = v^{\text{eff}} \rho^A + iG_0^A W_0^{\text{eff}}$ , where  $v^{\text{eff}} = W^R$ ,  $\rho^{\text{eff}} = \rho^A$ ,  $G_0^{\text{eff}} = G_0^A$ , and  $W_0^{\text{eff}} = W_0$  (the derivation is reported in Sec. 2 of the SI). The final result reads

$$\Sigma^{\text{dc}} = W_0^R \rho^A + iG_0^A W_0. \quad (24)$$

We note that in the second term of Eq. 24, the screened Coulomb potential in  $A$  is obtained

by adding to  $W_0^R$  the screening potential generated by the polarizability  $P_0^A$ . This addition yields by definition the total screened Coulomb potential, since  $W_0^{-1} = [W_0^R]^{-1} - P_0^A$ . We note that the chain rule by construction leads to a Hartree double-counting self-energy (the first term of Eq. 24) that is defined in terms of the partially screened Coulomb potential. This is essential to remove the Hartree self-energy of the effective Hamiltonian (see Sec. 2 in the SI) that is already accounted for in the  $G_0W_0$  calculation of the total system ( $A+E$ ). Equivalently, the second term in Eq. 24 removes the exchange-correlation self-energy of the effective Hamiltonian at the  $G_0W_0$  level, as this self-energy has already been accounted for in the  $G_0W_0$  calculation of the total system.

Having obtained explicit expressions for the double counting terms, we can finally determine the one-body parameters of the effective Hamiltonian. We write  $G^R$  as:

$$\begin{aligned} [G^R]^{-1} &= g^{-1} - [V_H + iG_0W_0] + [W_0^R(\omega = 0)\rho + iG_0^AW_0] \\ &= \omega - H^{\text{KS}} + V_{\text{xc}} + W_0^R\rho^A - iG_0^RW_0. \end{aligned} \quad (25)$$

By comparing the equation above with Eqs. 5 and 15, we obtain the double counting contribution to the effective one-body terms as:

$$t^{\text{dc}} = V_{\text{xc}} + W_0^R(\omega = 0)\rho^A - iG_0^RW_0. \quad (26)$$

In general, the one-body terms should be frequency-dependent, due to the frequency dependency of  $G_0^R(\omega)$  and  $W_0(\omega)$ . To obtain static expressions for the one-body terms, we evaluate  $iG_0^RW_0$  at the quasi-particle energies. More details are provided in Sec. 3.

As we will see in Sec. 4, the double counting scheme defined here yields more accurate results than the Hartree-Fock one, since it satisfies the chain rule by construction. On the contrary, the Hartree-Fock double counting scheme used in Ref. 36,37,39–42 does not satisfy the chain rule and thus may introduce errors originating from the separation between active space and environment. A derivation of the Hartree-Fock double counting within the Green's

function formalism is provided in the SI.

### 3 Implementation

The QDET method and the double counting scheme of Eq. 26 are implemented in the WEST<sup>43</sup> (Without Empty States) code, a massively parallel open-source code designed for large-scale MBPT calculations of complex condensed-phase systems, such as defective solids. In the WEST code, a separable form of  $W_0$  is obtained using the projected eigen-decomposition of the dielectric matrix (PDEP)<sup>43,44</sup> which avoids the inversion and storage of large dielectric matrices. Importantly, explicit summations over empty KS orbitals entering the expressions of  $P_0$  and  $G_0$  are eliminated using density functional perturbation theory (DFPT)<sup>45</sup> and the Lanczos method,<sup>46,47</sup> respectively. The implementation of  $W_0^R$  in WEST has been reported previously.<sup>37</sup> In the following, we focus on the implementation of the double counting term entering Eq. 26.

In our current implementation, the active space  $A$  is defined by a set of Kohn-Sham eigenstates, and  $G_0^R$  is given by

$$G_0^R(\mathbf{x}, \mathbf{x}'; \omega) = \sum_i^E \frac{\psi_i^{\text{KS}}(\mathbf{x}) \psi_i^{\text{KS}}(\mathbf{x}')}{\omega - \epsilon_i^{\text{KS}} + i\eta \text{sgn}(\epsilon_i^{\text{KS}} - \epsilon_F)}, \quad (27)$$

where  $E$  is the environment,  $\text{sgn}$  is the sign function and  $\epsilon_F$  is the Fermi energy. The term  $\Delta\Sigma_{\text{xc}} = iG_0^R W_0$  in Eq. 26 is given by

$$\Delta\Sigma_{\text{xc}}(\omega) = i \int \frac{d\omega'}{2\pi} G_0^R(\omega + \omega') W_0(\omega'), \quad (28)$$

where the integration is performed using a contour deformation technique.<sup>43,48,49</sup> Finally, to obtain static double counting terms, we evaluate Eq. 28 at the quasiparticle energies  $\epsilon_i^{\text{QP}}$ , *i.e.*,

$$[\Delta\Sigma_{\text{xc}}]_{ij} = \frac{1}{2} \text{Re} \left[ [\Delta\Sigma_{\text{xc}}]_{ij}(\epsilon_i^{\text{QP}}) + [\Delta\Sigma_{\text{xc}}]_{ij}(\epsilon_j^{\text{QP}}) \right], \quad (29)$$

where the quasi-particle energies are obtained by solving iteratively the equation  $\epsilon_i^{\text{QP}} = \epsilon_i^{\text{KS}} + \langle \psi_i^{\text{KS}} | \Sigma_{\text{xc}}(\epsilon_i^{\text{QP}}) - V_{\text{xc}} | \psi_i^{\text{KS}} \rangle$ . We note that Eq. 29 has also been used in Ref. 50 to implement the self-consistent *GW* method.

## 4 Results

### 4.1 Computational setup

The electronic structure of a supercell representing a defect within a periodic solid is initially obtained by restricted close-shell DFT calculations, with an optimized geometry from unrestricted open-shell calculations. We use the Quantum Espresso<sup>51</sup> code, with the PBE<sup>52</sup> or DDH functional,<sup>53</sup> SG15 norm-conserving pseudopotentials<sup>54</sup> and a 50 Ry kinetic energy cutoff for the plane wave basis set. Only the  $\Gamma$ -point is employed to sample the Brillouin zone of the supercell.

The selection of the defect orbitals defining the active space may be performed by manually identifying a set of KS eigenstates localized around the defect of interest<sup>36,37,40</sup> or by using Wannier functions.<sup>41</sup> However these procedures do not offer a systematic means to verify convergence as a function of the composition and size of the active space.

Here we introduce a localization factor, a scalar  $L_V$ , associated to each KS orbital:

$$L_V(\psi_n^{\text{KS}}) = \int_{V \subseteq \Omega} |\psi_n^{\text{KS}}(\mathbf{x})|^2 d\mathbf{x}, \quad (30)$$

where  $V$  is a chosen volume including the defect, smaller than the supercell volume  $\Omega$ . The value of  $L_V$  varies between 0 and 1. The active space for a given defect is then defined by those KS orbitals for which  $L_V$  is larger than a given threshold. Decreasing the value of the threshold allows for a systematic change in the composition and number of orbitals belonging to the active space.

In our calculations, the parameters of the effective Hamiltonian are obtained using con-

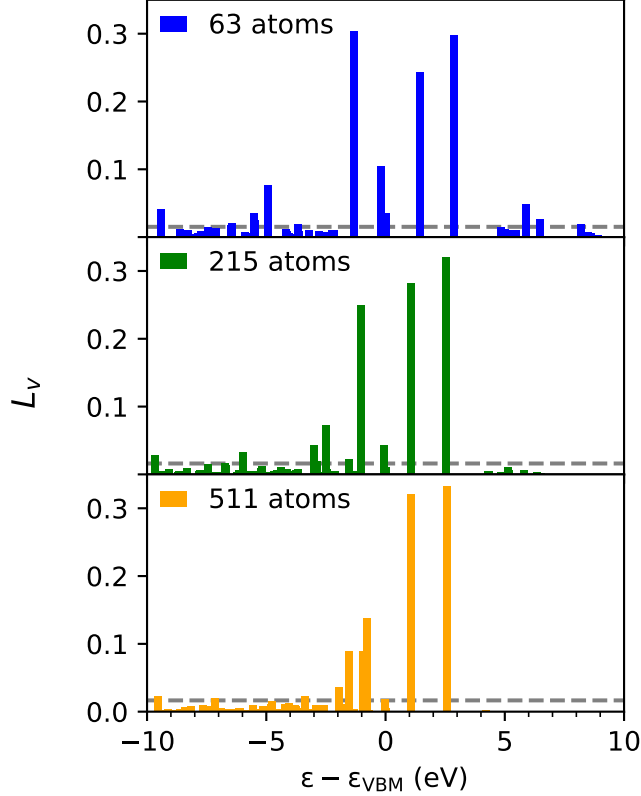


Figure 1: Localization factor ( $L_V$ , see Eq. 30) as a function of the energy of the Kohn-Sham orbitals, relative to the energy of the valence band maximum (VBM), for a  $\text{NV}^-$  center in diamond. We present results for supercells of three different sizes. The threshold used to define the active space is 5% (see text).

strained RPA (cRPA) calculations with the double counting correction of Eq. 26, called EDC@ $G_0W_0$ . The number of eigenpotentials  $N_{\text{PDEP}}$  used for the spectral decomposition of the polarizability is set to 512 in all calculations. Convergence tests as a function of  $N_{\text{PDEP}}$  are presented in Sec. 6 of the SI. Eigenvalues and eigenvectors of the active-space Hamiltonian are obtained with full-configuration interaction (FCI) calculations as implemented in the PySCF<sup>55</sup> code.

## 4.2 Negatively-charged nitrogen vacancy center in diamond

As a prototypical spin qubit for quantum information science,<sup>56–58</sup> the  $\text{NV}^-$  center in diamond has been extensively studied on different levels of theory.<sup>36,39,40,59–61</sup> It is generally

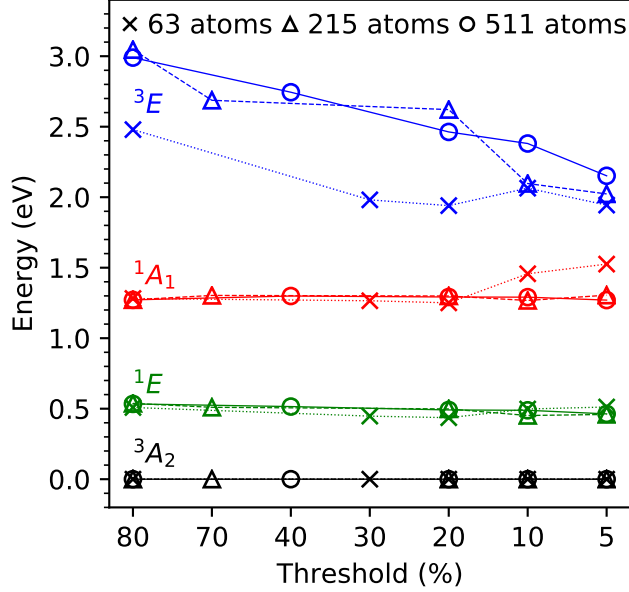


Figure 2: Computed vertical excitation energies of the  $\text{NV}^-$  center in diamond as a function of the chosen threshold of the localization factor  $L_V$  (see Eq. 30). States are labeled using the irreducible representation of the  $C_{3v}$  point group. We present results obtained with the PBE functional for cells of three different sizes. We note that 80% corresponds to a (4o, 6e), (3o, 4e) or (3o, 4e) active space for a 63-, 215- or 511-atom supercell respectively, and 5% corresponds to a (22o, 42e), (14o, 26e) or (12o, 22e) active space for a 63-, 215- or 511-atom supercell respectively.

recognized<sup>62,63</sup> that the four dangling bonds around the defect form a minimal model for the active space, with two non-degenerate  $a_1$  orbitals, and two degenerate orbitals with  $e$  character.

Instead of constructing a model with a priori knowledge of the defect electronic structure, we determine the active-space composition and size with the help of the localization factor defined in Eq. 30, as shown in Fig. 1. When using 63-, 215- and 511-atom supercells, irrespective of the threshold used to define  $L_V$ , we find three defect orbitals with energies within the band gap of diamond, corresponding to the two degenerate  $e$  orbitals and to one of the  $a_1$  orbital of the minimal model. In the 63- and 215-atom supercells, we find that one of the  $a_1$  orbitals belonging to the minimal model is below the VBM of diamond; in the 511-atom cell we find instead that three localized orbitals are below the VBM, indicating that at least 6 orbitals are required to define the active space. This suggests that the minimal



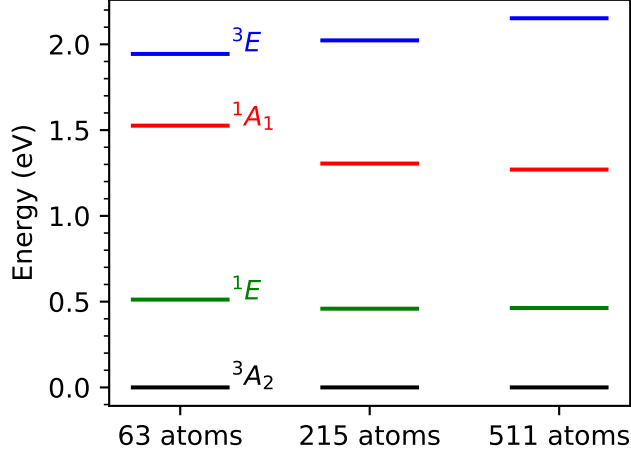


Figure 3: Computed vertical excitation energies for the  $\text{NV}^-$  in diamond. We show converged results (see Fig. 2) at 5% localization threshold as a function of the supercell size, obtained with the PBE functional.

model with a fixed number of orbitals may be insufficient to accurately describe the system with a large supercell.

In Fig. 2 we show the vertical excitation energies of the  $\text{NV}^-$  center obtained by diagonalizing the effective Hamiltonian (Eq. 1), as a function of the localization threshold chosen to define  $L_V$ . Irrespective of the chosen threshold, we find that the ground state has  ${}^3A_1$  symmetry. We also find that the lowest excited states with  ${}^1E$  and  ${}^1A_1$  symmetry converge much faster as a function of the  $L_V$  threshold than  ${}^3E$ , since  ${}^3E$  arises from  $a_1^1e^3$  configurations rather than a  $a_1^2e^2$  configurations, as in the case of  ${}^3A_2$ ,  ${}^1E$  and  ${}^1A_1$ . Most orbitals added to the active space when decreasing the localization threshold exhibit  $a_1$  character. We note that the convergence of the  ${}^1A_1$  state in the 63-atom cell is not smooth, probably due to orbitals with  $e$  character being part of the active space as the threshold value is decreased. Overall our results point at the need to converge the composition and size of the active space both as a function of  $L_V$  and cell size. In Fig. 3 we show the vertical excitation energies of the  $\text{NV}^-$  center as a function of supercell size, and the values are summarized in Tab. 1. We chose a 5%  $L_V$  threshold, i.e. all orbitals with  $L_V \geq 0.05$  are included in the active space  $A$ . As shown in Tab. 1, results obtained using the  $\text{EDC}@G_0W_0$  correction are much closer to the

experimental values than those computed using the original Hartree-Fock double counting correction (see Section 2.2.3), which we call here HFDC. Furthermore, we find unphysical excitations (i.e. states that do not have any experimental counterpart) with HFDC; however such unphysical states are not present when we use the EDC@ $G_0W_0$  correction (see Sec. 7.3 of the SI for details).

In our previous work, using HFDC corrections we found substantial differences between results obtained with the PBE or the hybrid functional DDH.<sup>53,64–68</sup> Hence we analyze the influence of the chosen functional when using the EDC@ $G_0W_0$  correction. In Fig. 4 and 5, we compare PBE and DDH results for the  $NV^-$  center, for converged active space in a 215-atom cell. Our results indicate that, except for a widening of the bandgap, the electronic structure is almost insensitive to the choice of the functional. The order of localized defect states within the gap and their localization properties are nearly identical when using PBE and DDH, and the shift of the position of the defect orbitals relative to the band edges is mostly due to the difference in the PBE and DDH bandgaps. The excitation energies of DDH calculations are less than 0.1 eV higher than their PBE counterparts. It is reasonable to expect that the insensitivity to the functional found here in the case of the  $NV^-$  center may apply more generally to other classes of covalently bonded semiconductors; it appears that the sensitivity observed with the HFDC scheme may have been caused by the incomplete double counting correction of the DFT exchange-correlation effects. However obtaining results for additional defects and solids will be necessary to come to a firm conclusion.

### 4.3 Neutral group-IV vacancy centers in diamond

In the last decade, a number of studies have investigated group-IV vacancy centers in diamond,<sup>36,40,76–80</sup> using either a four-orbital<sup>79</sup> or a nine-orbital minimal model.<sup>40</sup>

Similar to the case of the  $NV^-$  in diamond, we determine the active space using the localization factor shown in Fig. 6. We find a considerable number of localized orbitals. We exclude from the active space the localized conduction band orbitals, which are around 5 eV

Table 1: Computed vertical excitation energies (eV) for the  $\text{NV}^-$  in diamond for three states (see Fig. 3) obtained with QDET, the PBE functional and 511-atom supercells. We show results using the Hartree-Fock double counting (HFDC) and exact double counting (EDC@ $G_0W_0$ ) schemes (see text). We also report experimental results (Exp), including results for zero-phonon lines (ZPL), and results obtained using  $GW$  and the Bethe-Salpeter Equation (BSE), model fit from  $GW$  solved by configuration interaction (CI), model obtained from constrained random phase approximation (cRPA) solved by CI, and quantum chemistry results on clusters from complete active space self-consistent field (CASSCF), multireference configuration interaction (MRCI) and Monte Carlo configuration interaction (MCCI).

| Reference\Electronic States                                      | $^1E$     | $^1A_1$   | $^3E$ |
|--|-----------|-----------|-------|
| Exp <sup>56</sup>  |           |           | 2.18  |
| Exp ZPL <sup>56-58,69,70</sup>                                   | 0.34–0.43 | 1.51–1.60 | 1.945 |
| QDET (EDC@ $G_0W_0$ )  | 0.463     | 1.270     | 2.152 |
| QDET (HFDC)  | 0.375     | 1.150     | 1.324 |
| $GW$ + BSE <sup>71</sup>   | 0.40      | 0.99      | 2.32  |
| Model fit from $GW$ + CI <sup>61</sup>                           | 0.5       | 1.5       | 2.1   |
| Model from CRPA + CI <sup>39</sup>                               | 0.49      | 1.41      | 2.02  |
| $\text{C}_{85}\text{H}_{76}\text{N}^-$ CASSCF(6,6) <sup>72</sup> | 0.25      | 1.60      | 2.14  |
| $\text{C}_{49}\text{H}_{52}\text{N}^-$ CASSCF(6,8) <sup>73</sup> |           |           | 2.57  |
| $\text{C}_{19}\text{H}_{28}\text{N}^-$ MRCI(8,10) <sup>74</sup>  | 0.50      | 1.23      | 1.36  |
| $\text{C}_{42}\text{H}_{42}\text{N}^-$ MCCI <sup>75</sup>        | 0.63      | 2.06      | 1.96  |

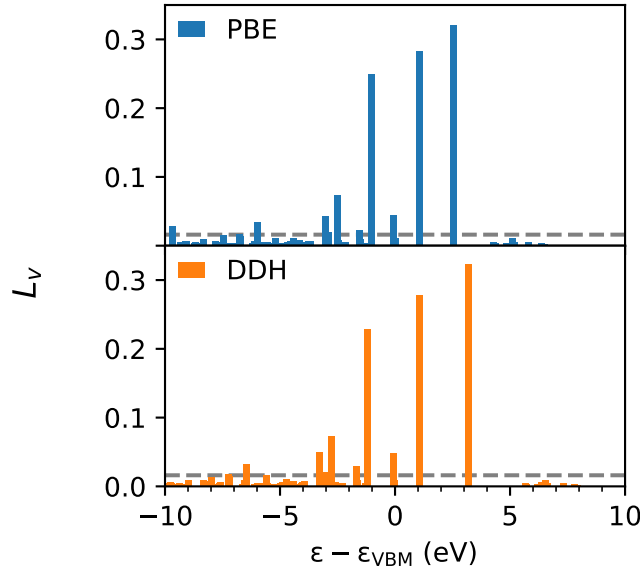


Figure 4: Localization factor ( $L_V$ , see Eq. 30) as a function of the energy of the Kohn-Sham orbitals, relative to the energy of the valence band maximum (VBM), for a  $\text{NV}^-$  center in diamond. We present results for 215-atom cell obtained with the PBE and DDH functionals. The threshold used to define the active space is 5% (see text).

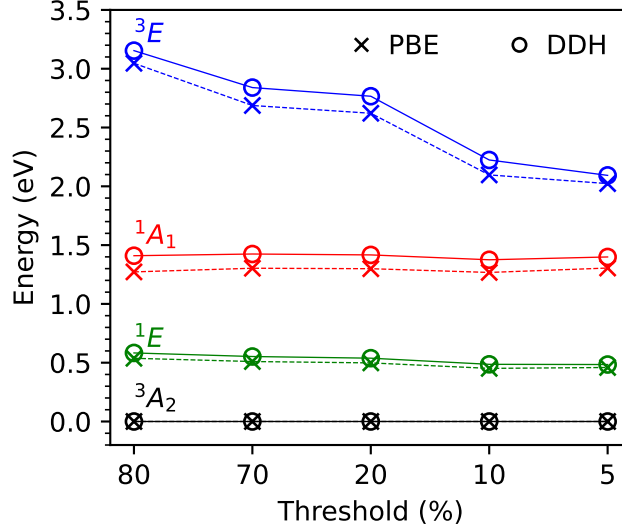


Figure 5: Computed vertical excitation energies of the  $\text{NV}^-$  center in diamond as a function of the chosen threshold of the localization factor  $L_V$  (see Eq. 30) to define the active space. States are labeled using the irreducible representation of the  $C_{3v}$  point group. We present results for 215-atom cell obtained with the PBE and DDH functionals. We note that 80% threshold corresponds to a (3o, 4e) active space, and 5% threshold corresponds to a (14o, 26e) or (15o, 28e) active space for PBE or DDH respectively.

in  $\text{SiV}^0$ , since we found their contribution to the excitation energies to be negligible (see Sec. 6 of the SI). We also exclude the defect atom’s strongly-bound atomic orbitals, present at about -20 eV in  $\text{GeV}^0$ ,  $\text{SnV}^0$  and  $\text{PbV}^0$ , which have almost no hybridization with the host orbitals.

The vertical excitation energies of  $\text{SiV}^0$  as a function of the localization threshold is reported in Fig. 7. In all three supercells we find a slow convergence of the excitation energies, indicating that the excited states of this system are the result of the combination of many single-particle orbitals, and that a minimal model may be insufficient to obtain reliable excitation energies. Using the converged excitation energies for a given supercell, we show the convergence with supercell size in Fig. 8. Similar to the case of the  $\text{NV}^-$  center, the low-energy excitations are well converged with a 63-atom supercell, while the convergence of the  ${}^3A_{2u}$ ,  ${}^3E_u$ ,  ${}^1A_{1u}$ , and  ${}^3A_{1u}$  states is slower. In Tab. 2, we compare our best converged values obtained with the  $\text{EDC}@G_0W_0$  correction with those obtained with

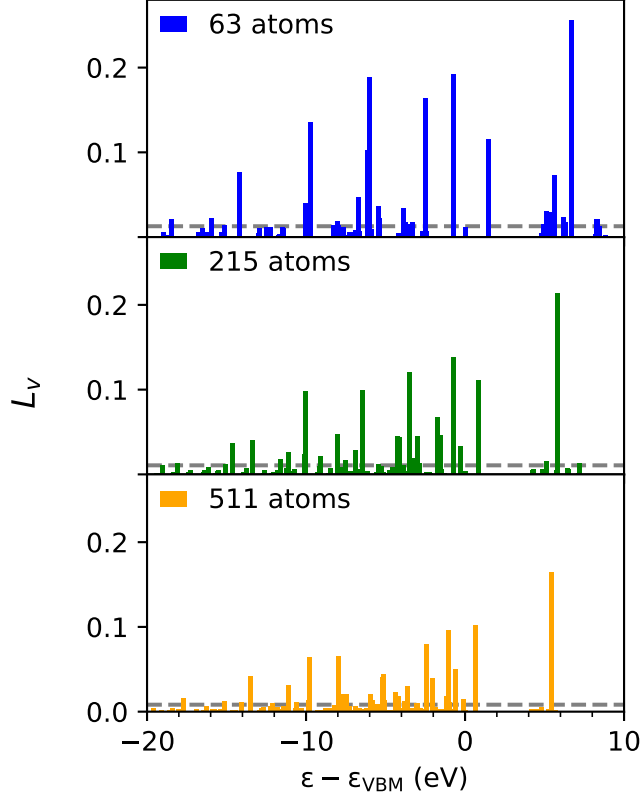


Figure 6: Localization factor ( $L_V$ , see Eq. 30) as a function of the energy of the Kohn-Sham orbitals, relative to the energy of the valence band maximum (VBM), for a  $\text{SiV}^0$  center in diamond. We present results for supercells of three different sizes. The threshold used to define the active space is 5% (see text).

the HFDC correction, as well as with available experimental and theoretical data. In general, the energies predicted using  $\text{EDC}@G_0W_0$  are higher than those obtained with HFDC, and in better agreement with those of quantum chemical cluster calculations.<sup>38</sup> We note that the experimental zero phonon line (ZPL) corresponding to the  ${}^3E_u$  level is 1.31 eV, but the contribution from the dynamical Jahn-Teller effect is unknown. Furthermore, the excitation energies computed with  $\text{EDC}@G_0W_0$  show faster convergence compared to those with HFDC. For example, using  $\text{EDC}@G_0W_0$  (HFDC) we find a difference of 0.15 (0.65) eV with 63-atom and 215-atom cells. As shown in Figs. 9 and 10, our results with the  $\text{EDC}@G_0W_0$  scheme showed insensitivity to the choice of the functional. Our results for  $\text{GeV}^0$ ,  $\text{SnV}^0$  and  $\text{PbV}^0$  are similar to those of  $\text{SiV}^0$  and are summarized in Tab. 2 as well as Tab. S1 in the SI.

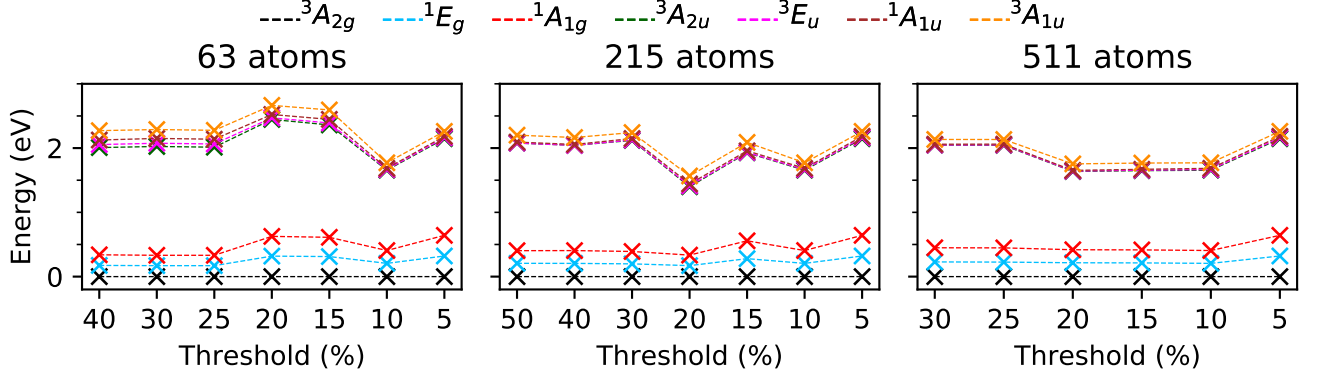


Figure 7: Computed vertical excitation energies of the  $\text{SiV}^0$  center in diamond as a function of the chosen threshold of the localization factor  $L_V$  (see Eq. 30) to define the active space. States are labeled using the irreducible representation of the  $D_{3d}$  point group. We present results obtained with the PBE functional for cells of three different sizes. We note that a 40%, 50% or 30% threshold corresponds to a (7o, 12e), (5o, 8e) or (9o, 16e) active space for a 63-, 215- or 511-atom supercell respectively, and 5% threshold corresponds to a (32o, 62e), (40o, 78e) or (48o, 94e) active space for a 63-, 215- or 511-atom supercell respectively.

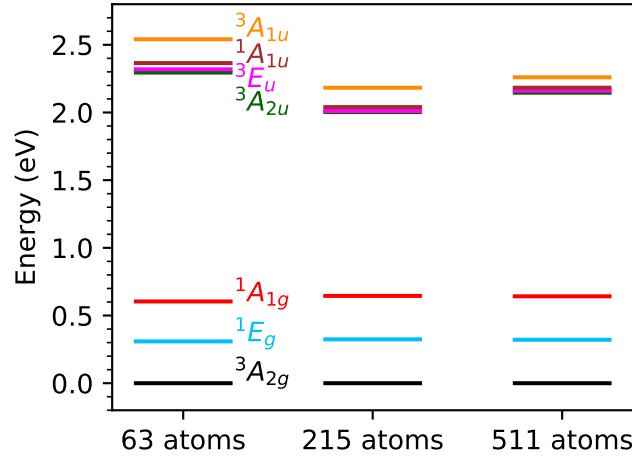


Figure 8: Computed vertical excitation energies for the  $\text{SiV}^0$  in diamond. We show converged results (see Fig. 2) at 5% localization threshold, as a function of the supercell size, obtained with the PBE functional.

## 5 Conclusions

In summary, in this work we presented a Green's function formulation of the quantum defect embedding theory (QDET) that enables the definition of an improved correction to the double counting scheme originally adopted in Refs 36,37. We defined an effective Hamiltonian

Table 2: Computed vertical excitation energies (eV) for the  $\text{SiV}^0$ ,  $\text{GeV}^0$ ,  $\text{SnV}^0$  and  $\text{PbV}^0$  in diamond for six states (see also Fig. 8 for the  $\text{SiV}^0$  results) obtained with QDET, the PBE functional and 511-atom supercells. We show results using the Hartree-Fock double counting (HFDC) and exact double counting (EDC@ $G_0W_0$ ) schemes (see text). We also report experimental results for zero-phonon lines (ZPL), and results obtained with a combination of second-order  $N$ -electron valence state perturbation theory (NEVPT2) and density matrix embedding theory (DMET), and quantum chemistry calculations on clusters from NEVPT2.

| System         | Reference\Electronic States   | $^1E_g$ | $^1A_{1g}$ | $^3A_{2u}$ | $^3E_u$ | $^1A_{1u}$ | $^3A_{1u}$ |
|----------------|---|---------|------------|------------|---------|------------|------------|
| $\text{SiV}^0$ | Exp ZPL   |         |            |            | 1.31    |            |            |
|                | QDET (EDC@ $G_0W_0$ )   | 0.321   | 0.642      | 2.146      | 2.161   | 2.183      | 2.260      |
|                | QDET (HFDC)   | 0.236   | 0.435      | 1.098      | 1.096   | 1.111      | 1.188      |
|                | NEVPT2-DMET(10,12) <sup>38</sup>                                    | 0.51    | 1.14       | 2.39       | 2.47    |            | 2.61       |
|                | $\text{C}_{84}\text{H}_{78}\text{Si}_0$ NEVPT2(10,12) <sup>38</sup> | 0.54    | 1.10       | 2.10       | 2.16    |            | 2.14       |
| $\text{GeV}^0$ | QDET (EDC@ $G_0W_0$ )   | 0.357   | 0.717      | 2.924      | 2.925   | 2.940      | 2.970      |
|                | QDET (HFDC)   | 0.289   | 0.554      | 1.456      | 1.443   | 1.443      | 1.495      |
| $\text{SnV}^0$ | QDET (EDC@ $G_0W_0$ )   | 0.295   | 0.596      | 2.590      | 2.571   | 2.561      | 2.616      |
|                | QDET (HFDC)   | 0.276   | 0.551      | 1.459      | 1.444   | 1.436      | 1.491      |
| $\text{PbV}^0$ | QDET (EDC@ $G_0W_0$ )   | 0.319   | 0.640      | 3.095      | 3.072   | 3.056      | 3.099      |
|                | QDET (HFDC)   | 0.302   | 0.600      | 1.788      | 1.768   | 1.755      | 1.796      |

for the active space within a Green’s function formalism, where the effective interaction is static and the self-energy cross-terms between the active space and the environment are neglected. Our results show that these approximations are appropriate to describe the localized defect states in semiconductors investigated in this work. Within the Green’s function formalism adopted here, we derived an exact double counting scheme (EDC@ $G_0W_0$ ) replacing the approximate scheme originally adopted in Refs 36,37. We emphasize that the double counting correction EDC@ $G_0W_0$  enables the removal of any double counting terms arising from the separation of the whole system into active space and environment. We then described the implementation of the scheme within the WEST code,<sup>43</sup> including a strategy to ensure convergence of our calculations with respect to the size and composition of the active space. Further, we demonstrated that QDET with exact double counting provides reliable results for several defects in diamond, with negligible dependence on the functional chosen for the underlying DFT calculations of the defects. Work is in progress to apply QDET with the EDC@ $G_0W_0$  scheme to more complex systems, such as defects in oxides and molecules

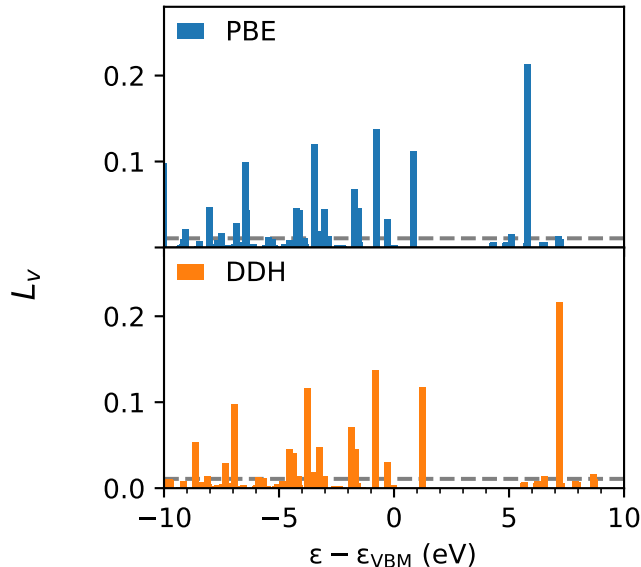


Figure 9: Localization factor ( $L_V$ , see Eq. 30) as a function of the energy of the Kohn-Sham orbitals, relative to the energy of the valence band maximum (VBM), for a  $\text{SiV}^0$  center in diamond. We present results for a 215-atom cell obtained with the PBE and DDH functionals. The threshold used to define the active space is 5% (see text).

on surfaces.

## Supporting information

Definition of matrix elements (section 1), comparison with other double counting schemes in the literature (section 2), implementation details (section 3), Hartree-Fock double counting (section 4), convergence of QDET calculations (section 5), discussion of ghost states (section 6), and a table of vertical excitation energies (section 7).

## Acknowledgements

This work was supported by MICCoM, as part of the Computational Materials Sciences Program funded by the U.S. Department of Energy, Office of Science, Basic Energy Sciences, Materials Sciences and Engineering Division through Argonne National Laboratory, under contract number DE-AC02-06CH11357. This research used resources of the National Energy



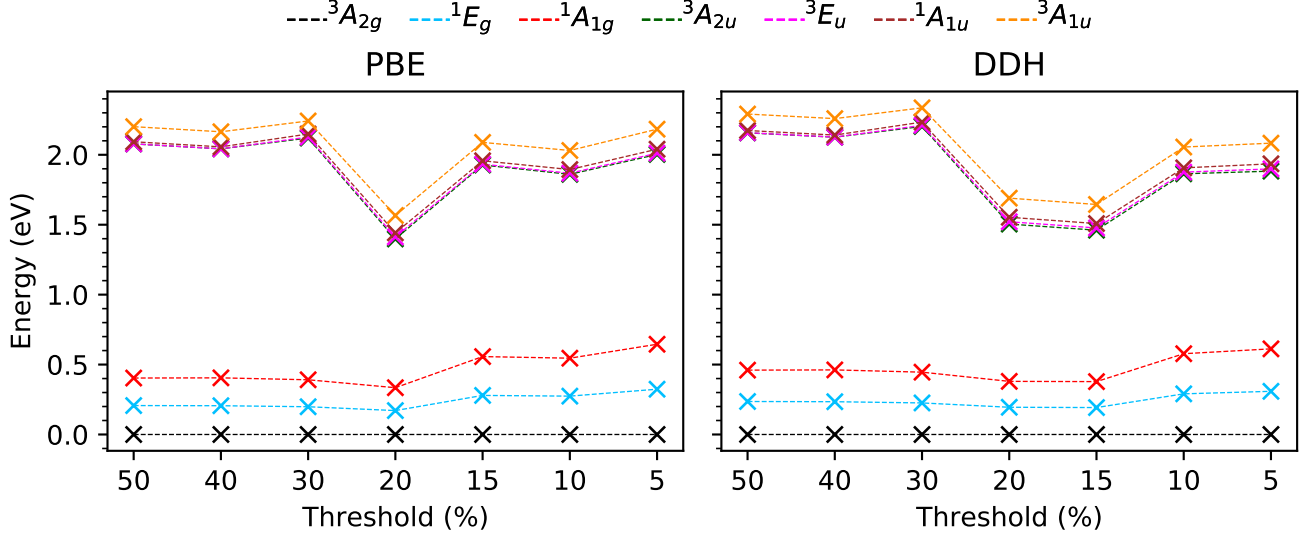


Figure 10: Computed vertical excitation energies (eV) of the  $\text{NV}^-$  center in diamond as a function of the chosen threshold of the localization factor  $L_V$  (see Eq. 30). States are labeled using the irreducible representation of the  $D_{3d}$  point group. We present results for a 215-atom cell obtained with the PBE and DDH functionals.

Research Scientific Computing Center (NERSC), a DOE Office of Science User Facility supported by the Office of Science of the US Department of Energy under Contract No. DE-AC02-05CH11231, and resources of the University of Chicago Research Computing Center.

## References

- (1) Hohenberg, P.; Kohn, W. Inhomogeneous Electron Gas. *Phys. Rev.* **1964**, *136*, B864–B871.
- (2) Kohn, W.; Sham, L. J. Self-Consistent Equations Including Exchange and Correlation Effects. *Phys. Rev.* **1965**, *140*, A1133–A1138.
- (3) Neugebauer, J.; Hickel, T. Density Functional Theory in Materials Science. *WIREs Computational Molecular Science* **2013**, *3*, 438–448.
- (4) Mardirossian, N.; Head-Gordon, M. Thirty Years of Density Functional Theory in Com-

- putational Chemistry: An Overview and Extensive Assessment of 200 Density Functionals. *Mol. Phys.* **2017**, *115*, 2315–2372.
- (5) Jones, R. O. Density Functional Theory: Its Origins, Rise to Prominence, and Future. *Rev. Mod. Phys.* **2015**, *87*, 897–923.
  - (6) Burke, K. Perspective on density functional theory. *J. Chem. Phys.* **2012**, *136*, 150901.
  - (7) Strinati, G. Application of the green’s functions method to the study of the optical properties of semiconductors. *Riv. Nuovo Cimento* **1988**, *11*, 1–86.
  - (8) Martin, R. M.; Reining, L.; Ceperley, D. M. *Interacting electrons*; Cambridge University Press, 2016.
  - (9) Golze, D.; Dvorak, M.; Rinke, P. The GW Compendium: A Practical Guide to Theoretical Photoemission Spectroscopy. *Front. Chem.* **2019**, *7*, 377.
  - (10) Bartlett, R. J.; Musiał, M. Coupled-Cluster Theory in Quantum Chemistry. *Rev. Mod. Phys.* **2007**, *79*, 291–352.
  - (11) Zhang, I. Y.; Grüneis, A. Coupled Cluster Theory in Materials Science. *Front. Mater.* **2019**, *6*.
  - (12) Helgaker, T.; Jorgensen, P.; Olsen, J. *Molecular electronic-structure theory*; John Wiley & Sons, 2014.
  - (13) Sun, Q.; Chan, G. K.-L. Quantum Embedding Theories. *Acc. Chem. Res.* **2016**, *49*, 2705–2712.
  - (14) Jones, L. O.; Mosquera, M. A.; Schatz, G. C.; Ratner, M. A. Embedding Methods for Quantum Chemistry: Applications from Materials to Life Sciences. *J. Am. Chem. Soc.* **2020**, *142*, 3281–3295.

- (15) Sheng, N.; Vorwerk, C.; Govoni, M.; Galli, G. Quantum Simulations of Material Properties on Quantum Computers. *arXiv:2105.04736 [cond-mat, physics:quant-ph]* **2021**, arXiv: 2105.04736.
- (16) Senn, H. M.; Thiel, W. QM/MM Methods for Biomolecular Systems. *Angew. Chem. Int. Ed.* **2009**, *48*, 1198–1229.
- (17) Liu, M.; Wang, Y.; Chen, Y.; Field, M. J.; Gao, J. QM/MM through the 1990s: The First Twenty Years of Method Development and Applications. *Isr. J. Chem.* **2014**, *54*, 1250–1263.
- (18) Libisch, F.; Huang, C.; Carter, E. A. Embedded Correlated Wavefunction Schemes: Theory and Applications. *Acc. Chem. Res.* **2014**, *47*, 2768–2775.
- (19) Gomes, A. S. P.; Jacob, C. R.; Visscher, L. Calculation of Local Excitations in Large Systems by Embedding Wave-Function Theory in Density-Functional Theory. *Phys. Chem. Chem. Phys.* **2008**, *10*, 5353–5362.
- (20) Goodpaster, J. D.; Barnes, T. A.; Manby, F. R.; Miller, T. F. Density Functional Theory Embedding for Correlated Wavefunctions: Improved Methods for Open-Shell Systems and Transition Metal Complexes. *J. Chem. Phys.* **2012**, *137*, 224113.
- (21) Wouters, S.; Jiménez-Hoyos, C. A.; Sun, Q.; Chan, G. K.-L. A Practical Guide to Density Matrix Embedding Theory in Quantum Chemistry. *J. Chem. Theory. Comput.* **2016**, *12*, 2706–2719.
- (22) Knizia, G.; Chan, G. K.-L. Density Matrix Embedding: A Simple Alternative to Dynamical Mean-Field Theory. *Phys. Rev. Lett.* **2012**, *109*, 186404.
- (23) Knizia, G.; Chan, G. K.-L. Density Matrix Embedding: A Strong-Coupling Quantum Embedding Theory. *J. Chem. Theory. Comput.* **2013**, *9*, 1428–1432.

- (24) Cui, Z.-H.; Zhu, T.; Chan, G. K.-L. Efficient Implementation of Ab Initio Quantum Embedding in Periodic Systems: Density Matrix Embedding Theory. **2020**, *16*, 119–129.
- (25) Pham, H. Q.; Hermes, M. R.; Gagliardi, L. Periodic Electronic Structure Calculations with the Density Matrix Embedding Theory. *J. Chem. Theory. Comput.* **2020**, *16*, 130–140.
- (26) Hermes, M. R.; Gagliardi, L. Multiconfigurational Self-Consistent Field Theory with Density Matrix Embedding: The Localized Active Space Self-Consistent Field Method. *J. Chem. Theory. Comput.* **2019**, *15*, 972–986.
- (27) Pham, H. Q.; Bernales, V.; Gagliardi, L. Can Density Matrix Embedding Theory with the Complete Activate Space Self-Consistent Field Solver Describe Single and Double Bond Breaking in Molecular Systems? *J. Chem. Theory. Comput.* **2018**, *14*, 1960–1968.
- (28) Lan, T. N.; Zgid, D. Generalized Self-Energy Embedding Theory. *J. Chem. Phys. Lett.* **2017**, *8*, 2200–2205.
- (29) Zgid, D.; Gull, E. Finite Temperature Quantum Embedding Theories for Correlated Systems. *New. J. Phys.* **2017**, *19*, 023047.
- (30) Rusakov, A. A.; Iskakov, S.; Tran, L. N.; Zgid, D. Self-Energy Embedding Theory (SEET) for Periodic Systems. *J. Chem. Theory. Comput.* **2019**, *15*, 229–240.
- (31) Georges, A.; Kotliar, G. Hubbard Model in Infinite Dimensions. *Phys. Rev. B* **1992**, *45*, 6479–6483.
- (32) Georges, A.; Kotliar, G.; Krauth, W.; Rozenberg, M. J. Dynamical Mean-Field Theory of Strongly Correlated Fermion Systems and the Limit of Infinite Dimensions. *Rev. Mod. Phys.* **1996**, *68*, 13–125.

- (33) Georges, A. Strongly Correlated Electron Materials: Dynamical Mean-Field Theory and Electronic Structure. *AIP Conf. Proc.* **2004**, *715*, 3–74.
- (34) Anisimov, V. I.; Poteryaev, A. I.; Korotin, M. A.; Anokhin, A. O.; Kotliar, G. First-Principles Calculations of the Electronic Structure and Spectra of Strongly Correlated Systems: Dynamical Mean-Field Theory. *J. Phys. Condens. Matter.* **1997**, *9*, 7359–7367.
- (35) Kotliar, G.; Savrasov, S. Y.; Haule, K.; Oudovenko, V. S.; Parcollet, O.; Marianetti, C. A. Electronic Structure Calculations with Dynamical Mean-Field Theory. *Rev. Mod. Phys.* **2006**, *78*, 865–951.
- (36) Ma, H.; Govoni, M.; Galli, G. Quantum Simulations of Materials on Near-Term Quantum Computers. *npj Comput. Mater.* **2020**, *6*, 1–8.
- (37) Ma, H.; Sheng, N.; Govoni, M.; Galli, G. Quantum Embedding Theory for Strongly Correlated States in Materials. *J. Chem. Theory. Comput.* **2021**, *17*, 2116–2125.
- (38) Mitra, A.; Pham, H. Q.; Pandharkar, R.; Hermes, M. R.; Gagliardi, L. Excited States of Crystalline Point Defects with Multireference Density Matrix Embedding Theory. *J. Phys. Chem. Lett.* **2021**, *12*, 11688–11694.
- (39) Bockstedte, M.; Schütz, F.; Garratt, T.; Ivády, V.; Gali, A. Ab initio description of highly correlated states in defects for realizing quantum bits. *npj Quantum Mater.* **2018**, *3*, 1–6.
- (40) Ma, H.; Sheng, N.; Govoni, M.; Galli, G. First-Principles Studies of Strongly Correlated States in Defect Spin Qubits in Diamond. *Phys. Chem. Chem. Phys.* **2020**, *22*, 25522–25527.
- (41) Muechler, L.; Badrtdinov, D. I.; Hampel, A.; Cano, J.; Rösner, M.; Dreyer, C. E. Quan-

- tum embedding methods for correlated excited states of point defects: Case studies and challenges. *arXiv:2105.08705 [cond-mat]* **2021**, arXiv: 2105.08705.
- (42) Pfäffle, W.; Antonov, D.; Wrachtrup, J.; Bester, G. Screened configuration interaction method for open-shell excited states applied to NV centers. *Phys. Rev. B* **2021**, *104*, 104105.
  - (43) Govoni, M.; Galli, G. Large Scale GW Calculations. *J. Chem. Theory. Comput.* **2015**, *11*, 2680–2696.
  - (44) Wilson, H. F.; Gygi, F.; Galli, G. Efficient iterative method for calculations of dielectric matrices. *Phys. Rev. B* **2008**, *78*, 113303.
  - (45) Baroni, S.; de Gironcoli, S.; Dal Corso, A.; Giannozzi, P. Phonons and Related Crystal Properties from Density-Functional Perturbation Theory. *Rev. Mod. Phys.* **2001**, *73*, 515–562.
  - (46) Umari, P.; Stenuit, G.; Baroni, S. GW quasiparticle spectra from occupied states only. *Phys. Rev. B* **2010**, *81*, 115104.
  - (47) Nguyen, H.-V.; Pham, T. A.; Rocca, D.; Galli, G. Improving Accuracy and Efficiency of Calculations of Photoemission Spectra within the Many-Body Perturbation Theory. *Phys. Rev. B* **2012**, *85*, 081101.
  - (48) Godby, R. W.; Schlüter, M.; Sham, L. J. Self-Energy Operators and Exchange-Correlation Potentials in Semiconductors. *Phys. Rev. B* **1988**, *37*, 10159–10175.
  - (49) Giantomassi, M.; Stankovski, M.; Shaltaf, R.; Grüning, M.; Bruneval, F.; Rinke, P.; Rignanese, G.-M. Electronic Properties of Interfaces and Defects from Many-Body Perturbation Theory: Recent Developments and Applications. *Phys. Status Solidi B* **2011**, *248*, 275–289.

- (50) van Schilfgaarde, M.; Kotani, T.; Faleev, S. Quasiparticle Self-Consistent G W Theory. *Phys. Rev. Lett.* **2006**, *96*, 226402.
- (51) Giannozzi, P.; Baroni, S.; Bonini, N.; Calandra, M.; Car, R.; Cavazzoni, C.; Ceresoli, D.; Chiarotti, G. L.; Cococcioni, M.; Dabo, I.; Corso, A. D.; de Gironcoli, S.; Fabris, S.; Fratesi, G.; Gebauer, R.; Gerstmann, U.; Gougoussis, C.; Kokalj, A.; Lazzeri, M.; Martin-Samos, L.; Marzari, N.; Mauri, F.; Mazzarello, R.; Paolini, S.; Pasquarello, A.; Paulatto, L.; Sbraccia, C.; Scandolo, S.; Sclauzero, G.; Seitsonen, A. P.; Smogunov, A.; Umari, P.; Wentzcovitch, R. M. QUANTUM ESPRESSO: a modular and open-source software project for quantum simulations of materials. *J. Phys.: Condens. Matter* **2009**, *21*, 395502.
- (52) Perdew, J. P.; Burke, K.; Ernzerhof, M. Generalized Gradient Approximation Made Simple. *Phys. Rev. Lett.* **1996**, *77*, 3865–3868.
- (53) Skone, J. H.; Govoni, M.; Galli, G. Self-consistent hybrid functional for condensed systems. *Phys. Rev. B* **2014**, *89*, 195112.
- (54) Schlipf, M.; Gygi, F. Optimization algorithm for the generation of ONCV pseudopotentials. *Comput. Phys. Commun.* **2015**, *196*, 36–44.
- (55) Sun, Q.; Berkelbach, T. C.; Blunt, N. S.; Booth, G. H.; Guo, S.; Li, Z.; Liu, J.; McClain, J. D.; Sayfutyarova, E. R.; Sharma, S.; Wouters, S.; Chan, G. K.-L. PySCF: The Python-Based Simulations of Chemistry Framework. *WIREs Comput. Mol. Sci.* **2018**, *8*, e1340.
- (56) Davies, G.; Hamer, M. F.; Price, W. C. Optical Studies of the 1.945 eV Vibronic Band in Diamond. *Proc. R. Soc. London A* **1976**, *348*, 285–298.
- (57) Rogers, L. J.; Armstrong, S.; Sellars, M. J.; Manson, N. B. Infrared emission of the NV centre in diamond: Zeeman and uniaxial stress studies. *New J. Phys.* **2008**, *10*, 103024.

- (58) Goldman, M. L.; Sipahigil, A.; Doherty, M. W.; Yao, N. Y.; Bennett, S. D.; Markham, M.; Twitchen, D. J.; Manson, N. B.; Kubanek, A.; Lukin, M. D. Phonon-Induced Population Dynamics and Intersystem Crossing in Nitrogen-Vacancy Centers. *Phys. Rev. Lett.* **2015**, *114*, 145502.
- (59) Doherty, M. W.; Manson, N. B.; Delaney, P.; Hollenberg, L. C. L. The negatively charged nitrogen-vacancy centre in diamond: the electronic solution. *New J. Phys.* **2011**, *13*, 025019.
- (60) Maze, J. R.; Gali, A.; Togan, E.; Chu, Y.; Trifonov, A.; Kaxiras, E.; Lukin, M. D. Properties of nitrogen-vacancy centers in diamond: the group theoretic approach. *New J. Phys.* **2011**, *13*, 025025.
- (61) Choi, S.; Jain, M.; Louie, S. G. Mechanism for optical initialization of spin in NV-center in diamond. *Phys. Rev. B* **2012**, *86*, 041202.
- (62) Loubser, J. H. N.; van Wyk, J. A. Electron Spin Resonance in the Study of Diamond. *Rep. Prog. Phys.* **1978**, *41*, 1201–1248.
- (63) Doherty, M. W.; Manson, N. B.; Delaney, P.; Jelezko, F.; Wrachtrup, J.; Hollenberg, L. C. The nitrogen-vacancy colour centre in diamond. *Phys. Rep.* **2013**, *528*, 1–45.
- (64) Skone, J. H.; Govoni, M.; Galli, G. Nonempirical range-separated hybrid functionals for solids and molecules. *Phys. Rev. B* **2016**, *93*, 235106.
- (65) Brawand, N. P.; Vörös, M.; Govoni, M.; Galli, G. Generalization of Dielectric-Dependent Hybrid Functionals to Finite Systems. *Phys. Rev. X* **2016**, *6*, 041002.
- (66) Brawand, N. P.; Govoni, M.; Vörös, M.; Galli, G. Performance and Self-Consistency of the Generalized Dielectric Dependent Hybrid Functional. *J. Chem. Theory Comput.* **2017**, *13*, 3318–3325, PMID: 28537727.



- (67) Gerosa, M.; Bottani, C. E.; Valentin, C. D.; Onida, G.; Pacchioni, G. Accuracy of dielectric-dependent hybrid functionals in the prediction of optoelectronic properties of metal oxide semiconductors: a comprehensive comparison with many-body GW and experiments. *J. Phys.: Condens. Matter* **2017**, *30*, 044003.
- (68) Zheng, H.; Govoni, M.; Galli, G. Dielectric-dependent hybrid functionals for heterogeneous materials. *Phys. Rev. Materials* **2019**, *3*, 073803.
- (69) Kehayias, P.; Doherty, M. W.; English, D.; Fischer, R.; Jarmola, A.; Jensen, K.; Leefer, N.; Hemmer, P.; Manson, N. B.; Budker, D. Infrared Absorption Band and Vibronic Structure of the Nitrogen-Vacancy Center in Diamond. *Phys. Rev. B* **2013**, *88*, 165202.
- (70) Goldman, M. L.; Doherty, M. W.; Sipahigil, A.; Yao, N. Y.; Bennett, S. D.; Manson, N. B.; Kubanek, A.; Lukin, M. D. State-Selective Intersystem Crossing in Nitrogen-Vacancy Centers. *Phys. Rev. B* **2015**, *91*, 165201.
- (71) Ma, Y.; Rohlfing, M.; Gali, A. Excited States of the Negatively Charged Nitrogen-Vacancy Color Center in Diamond. *Phys. Rev. B* **2010**, *81*, 041204.
- (72) Bhandari, C.; Wysocki, A. L.; Economou, S. E.; Dev, P.; Park, K. Multiconfigurational Study of the Negatively Charged Nitrogen-Vacancy Center in Diamond. *Phys. Rev. B* **2021**, *103*, 014115.
- (73) Lin, C.-K.; Wang, Y.-H.; Chang, H.-C.; Hayashi, M.; Lin, S. H. One- and Two-Photon Absorption Properties of Diamond Nitrogen-Vacancy Defect Centers: A Theoretical Study. *J. Chem. Phys.* **2008**, *129*, 124714.
- (74) Zyubin, A. S.; Mebel, A. M.; Hayashi, M.; Chang, H. C.; Lin, S. H. Quantum Chemical Modeling of Photoadsorption Properties of the Nitrogen-Vacancy Point Defect in Diamond. *J. Comput. Chem.* **2009**, *30*, 119–131.

- (75) Delaney, P.; Greer, J. C.; Larsson, J. A. Spin-Polarization Mechanisms of the Nitrogen-Vacancy Center in Diamond. *Nano Lett.* **2010**, *10*, 610–614.
- (76) Gali, A.; Maze, J. R. Ab initio study of the split silicon-vacancy defect in diamond: Electronic structure and related properties. *Phys. Rev. B* **2013**, *88*, 235205.
- (77) Thiering, G. m. H.; Gali, A. Ab Initio Magneto-Optical Spectrum of Group-IV Vacancy Color Centers in Diamond. *Phys. Rev. X* **2018**, *8*, 021063.
- (78) Green, B. L.; Doherty, M. W.; Nako, E.; Manson, N. B.; D’Haenens-Johansson, U. F. S.; Williams, S. D.; Twitchen, D. J.; Newton, M. E. Electronic Structure of the Neutral Silicon-Vacancy Center in Diamond. *Phys. Rev. B* **2019**, *99*, 161112.
- (79) Thiering, G.; Gali, A. The  $(eg \otimes eu) \otimes Eg$  product Jahn–Teller effect in the neutral group-IV vacancy quantum bits in diamond. *npj Comput. Mater.* **2019**, *5*, 18.
- (80) Zhang, Z.-H.; Stevenson, P.; Thiering, G.; Rose, B. C.; Huang, D.; Edmonds, A. M.; Markham, M. L.; Lyon, S. A.; Gali, A.; de Leon, N. P. Optically Detected Magnetic Resonance in Neutral Silicon Vacancy Centers in Diamond via Bound Exciton States. *Phys. Rev. Lett.* **2020**, *125*, 237402.

# Supporting Information for Green’s function formulation of quantum defect embedding theory

Nan Sheng,<sup>†,§</sup> Christian Vorwerk,<sup>‡,§</sup> Marco Govoni,<sup>\*,‡,¶</sup> and Giulia Galli<sup>\*,‡,†,¶</sup>

<sup>†</sup>*Department of Chemistry, University of Chicago, Chicago, IL 60637, USA.*

<sup>‡</sup>*Pritzker School of Molecular Engineering, University of Chicago, Chicago, IL 60637, USA.*

<sup>¶</sup>*Materials Science Division and Center for Molecular Engineering, Argonne National  
Laboratory, Lemont, IL 60439, USA.*

<sup>§</sup>*These two authors contributed equally.*

E-mail: mgovoni@anl.gov; gagalli@uchicago.edu

## 1 Definition of matrix elements

In the main text, matrix elements are given in a short-hand notation. Here, we provide detailed expressions of these matrix elements.

Matrix elements of the Hartree energy are given by

$$[V_{\text{H}}]_{ij} = [v\rho]_{ij} = \sum_{kl} v_{ikjl} \rho_{kl}, \quad (1)$$

where the matrix elements of the bare Coulomb potential  $v$ ,  $v_{ikjl}$ , are defined in Eq. 2 of the main text. Analogously, the matrix elements of the Hartree contribution to the double

counting term in Eq. 25 and 26 of the main text are given by

$$[W_0^R(\omega = 0)\rho^A]_{ij} = \sum_{kl}^A [W_0^R(\omega = 0)]_{ikjl} \rho_{kl}^A. \quad (2)$$

Here,  $\rho_{kl}$  are the matrix elements of the density matrix. The matrix elements of the  $G_0W_0$ -contribution to the self-energy in Eq. 26 are defined as<sup>1</sup>

$$[iG_0^RW_0]_{ij}(\omega) = i\langle\zeta_i|\int\frac{d\omega'}{2\pi}G_0^R(\mathbf{r},\mathbf{r}';\omega+\omega')W_0(\mathbf{r},\mathbf{r}';\omega')|\zeta_j\rangle, \quad (3)$$

where  $\zeta_i$  are the single-particle functions that span the active space. The reduced Kohn-Sham Green's function  $G_0^R$  is defined in Eq. 23 of the main text, the screened Coulomb potential  $W_0$  in Eq. 19.

## 2 Self-energy of the effective Hamiltonian

In this section, we derive the Hartree, Hartree-Fock, and  $G_0W_0$  self-energies for the effective Hamiltonian. The effective Hamiltonian is given by

$$H^{\text{eff}} = \sum_{ij}^A t_{ij}^{\text{eff}} a_i^\dagger a_j + \frac{1}{2} \sum_{ijkl}^A v_{ijkl}^{\text{eff}} a_i^\dagger a_j^\dagger a_l a_k, \quad (4)$$

where  $t^{\text{eff}}$  and  $v^{\text{eff}}$  are the effective one- and two-body terms, respectively. In the following, we assume that the active space is formed by a set of Kohn-Sham eigenstates. In this case, the independent-particle Green's function associated to the effective Hamiltonian  $G_0^{\text{eff}}$  is given by  $G_0^A$ . The density matrix  $\rho^{\text{eff}}$  associated to the effective Hamiltonian is given by  $\rho^A$ , which is the Kohn-Sham density matrix projected onto  $A$ .

The Hartree self-energy  $\Sigma_{\text{H}}^{\text{eff}}$  of the effective Hamiltonian is given by

$$\Sigma_{\text{H}}^{\text{eff}} = v^{\text{eff}} \rho^{\text{eff}} = v^{\text{eff}} \rho^A. \quad (5)$$

We note that  $v^{\text{eff}}$  is a renormalized Coulomb interaction that contains the effect of the screening generated by the electrons in the environment, but not the screening generated by the electrons in the active space.

### 2.1 Hartree-Fock

In the Hartree-Fock (HF) approximation, the polarizability is assumed to vanish, *i.e.*  $P_0^{\text{eff}} \approx 0$ , such that the interaction is not screened by the electrons that belong to the active space, *i.e.*  $W_0^{\text{eff}} = v^{\text{eff}}$ . Consequently, the Hartree-Fock self-energy of the effective Hamiltonian is given by

$$\Sigma_{\text{HF}}^{\text{eff}} = \Sigma_{\text{H}}^{\text{eff}} + \Sigma_{\text{x}}^{\text{eff}} = \Sigma_{\text{H}}^{\text{eff}} + iG_0^{\text{eff}} v^{\text{eff}} = v^{\text{eff}} \rho^A + iG_0^A v^{\text{eff}}, \quad (6)$$

where we employ the matrix notations of Eqs. 1 and 2.

## 2.2 $G_0W_0$

In the  $G_0W_0$  approximation, the screening generated by the electrons in the active space is described the effective polarizability  $P^{\text{eff}}$ . Within the the random-phase approximation,  $P^{\text{eff}} \approx P_0^{\text{eff}} = P_0^A$ . The screened potential is therefore  $W_0^{\text{eff}} = \left[ [v^{\text{eff}}]^{-1} - P_0^A \right]^{-1}$ , which includes the screening generated by the electrons in the environment (included in  $v^{\text{eff}}$ ) and the screening generated by the electrons in the active space (included in  $P_0^A$ ). As a result, the self-energy in the  $G_0W_0$  approximation is given by

$$\Sigma_{G_0W_0}^{\text{eff}} = \Sigma_{\text{H}}^{\text{eff}} + iG_0^{\text{eff}}W_0^{\text{eff}} = v^{\text{eff}}\rho^A + iG_0^A W_0^{\text{eff}}. \quad (7)$$

## 3 Exact double counting at Hartree-Fock level of theory (EDC@HF)

In the following, we derive a double counting term for the embedding of an active space into an environment that is described within the Hartree-Fock (HF) level of theory. Our derivation is analogous to the case of embedding in DFT+ $G_0W_0$  used in the main manuscript. To derive the double counting terms  $\Sigma^{\text{dc}}$  and  $P^{\text{dc}}$  in this case, we again require that the chain rule be satisfied, *i.e.*, that the self-energy and polarizability of the whole system ( $A + E$ ), evaluated at the low-level of theory, be identical to that of  $A$  embedded in  $E$ . Within the HF approximation this requirement yields

$$\Sigma^{\text{dc}} = \Sigma_{\text{HF}}^{\text{eff}} \quad (8)$$

$$P^{\text{dc}} = P_0^{\text{eff}}. \quad (9)$$

Within HF we have that  $P_0 = 0$  and  $W_0^R = v$ . Hence, the effective interaction in the active space is given by the bare Coulomb potential, *i.e.*  $v^{\text{eff}} = v$ .

The double counting contribution to the self-energy,  $\Sigma^{\text{dc}}$  is obtained by inserting the HF

self-energy of the effective Hamiltonian (Eq. 6) into the double-counting expression in Eq. 8. We thus obtain

$$\Sigma^{\text{dc}} = v\rho^A + iG_0^A v. \quad (10)$$

Having obtained explicit expressions for the double counting terms, we can finally determine the one-body parameters of the effective Hamiltonian. We write  $G^R$  as

$$\begin{aligned} [G^R]^{-1} &= g^{-1} - [V_{\text{H}} + iG_0 v] + [v\rho^A + iG_0^A v] \\ &= \omega - H^{\text{HF}} + v\rho^A + iG_0^A v \end{aligned} \quad (11)$$

From the equation above, we obtain the double counting contribution to the effective one-body terms in the HF scheme:

$$t^{\text{dc}} = v\rho^A + iG_0^A v. \quad (12)$$

By definition, this HF double counting correction — when applied to HF — satisfies the chain rule and hence it does not introduce errors that originate from the separation of the system into active space and the environment.

However, the HF double counting (HFDC) term used in Ref. 2–5, and reported in Eq. 6 of the main manuscript, contains two inconsistencies. The first inconsistency is given by the fact that the double-counting term is inspired by HF but is applied to DFT, hence leading to an approximate cancellation of double counting effects. Additionally, the polarizability is computed at the RPA level of theory and thus a screened Coulomb interaction instead of the bare Coulomb interaction is used. Instead, the double counting scheme discussed in the main text can be applied to DFT and consistently applies  $G_0W_0$  to the mean-field electronic structure.

## 4 Comparison with other double counting schemes in the literature

In this section, we compare the double counting (DC) scheme introduced in the main text to schemes adopted in other Green's function embedding theories including dynamical mean-field theory. To simplify the comparison, we consider the case of an active space composed of a set of localized correlated orbitals within the environment of a solid or condensed system whose Brillouin zone (BZ) is sampled by the  $\Gamma$ -point only. In dynamical mean-field theory (DMFT),<sup>6–10</sup> *local* quantities are defined as an average over  $\mathbf{k}$ -point, *e.g.*  $\Sigma^{\text{loc}} = \frac{1}{N_{\mathbf{k}}} \sum_{\mathbf{k}} \Sigma(\mathbf{k})$  and the *non-local* quantities as the remainders, *e.g.*  $\Sigma^{\text{non-loc}}(\mathbf{k}) = \Sigma(\mathbf{k}) - \Sigma^{\text{loc}}$ . In supercells with  $\Gamma$ -point sampling, every quantity is local by definition (all non-local contributions vanish).

### 4.1 Dynamical mean-field theory (DMFT)

We denote with DMFT+ $GW$ <sup>11–16</sup> a group of quantum-embedding methodologies that combine dynamical mean-field theory (DMFT) to describe the active space with the  $GW$  approximation for the environment. In this case, the self energy is expressed as<sup>17</sup>

$$\Sigma = \Sigma^{\text{DMFT}} + \Sigma^{\text{GW}} - \Sigma^{\text{dc}}, \quad (13)$$

where the double counting contribution  $\Sigma^{\text{dc}}$  is given by<sup>17,18</sup>

$$\Sigma^{\text{dc}} = G^{\text{loc},A} W^{\text{loc}}. \quad (14)$$

As mentioned above, when the Brillouin zone of the supercell is sampled solely with the  $\Gamma$ -point, all quantities are local. Hence, using  $G^A = f^A G f^A$ , it is easy to show that the double counting adopted within DMFT+ $GW$  is identical to the one derived in Eq. 26 in the main text.



We note that a double counting correction for DMFT+ $GW$  different to the one in Eq. 14,  $\Sigma^{\text{dc}2}$ , has been suggested in Refs.,<sup>17,18</sup> given by

$$\Sigma^{\text{dc}2} = \Sigma^{\text{loc},A} \neq G^{\text{loc},A} W^{\text{loc}}. \quad (15)$$

In this case, the projection on the subspace  $A$  is performed after the calculation of the self energy, and  $\Sigma^{\text{dc}2}$  contains contribution from the environment as well. Using the definition of  $\Sigma$  in the  $GW$  approximation,

$$\Sigma_{kl}(\tau) = - \sum_{mn}^{A+E} G_{mn}(\tau) W_{mknl}(\tau), \quad (16)$$

where  $\tau$  is the imaginary time,  $\Sigma^{\text{dc}2}$  is given by

$$\begin{aligned} \Sigma_{kl}^{\text{dc}2} &= f^A \sum_{mn}^{A+E} G_{mn} W_{mknl} f^A \\ &= f^A \sum_m^A G_{mm} W_{mkml} f^A + f^A \sum_m^E G_{mm} W_{mkml} f^A \\ &= \Sigma^{\text{dc}} + f^A \sum_m^E G_{mm} W_{mkml} f^A, \end{aligned} \quad (17)$$

where we took into account that the Green's function is diagonal in the single-particle space within the quasiparticle approximation. Equation 17 shows that  $\Sigma^{\text{dc}2}$  differs from  $\Sigma^{\text{dc}}$  by an additional term with an explicit summation over states in the environment  $E$ . While Ref.<sup>17</sup> initially found that there was no numerical difference between  $\Sigma^{\text{dc}}$  and  $\Sigma^{\text{dc}2}$  in DMFT+ $GW$  calculations, Ref.<sup>18</sup> later showed that  $\Sigma^{\text{dc}2}$  corrects non-causal contributions in the embedding of DMFT and quasiparticle self-consistent  $GW$  (DMFT+QSGW). We note that  $\Sigma^{\text{dc}2}$  violates the chain rule.

## 4.2 Extended dynamical mean-field theory (EDMFT)

While in DMFT the interaction in the active space is described by a set of Hubbard parameters, extended dynamical mean-field theory (EDMFT)<sup>15,16,19</sup> includes dynamical non-local correlation into the self-consistent solution of the auxiliary problem. Therefore, in EDMFT not only the local self-energy and Green's function are updated in the self-consistency cycle, but also the local polarizability and screened Coulomb potential. In EDMFT+*GW*, the self energy is expressed as<sup>15</sup>

$$\Sigma_{kl}^{\text{EDMFT}+GW} = \Sigma_{kl}^{\text{EDMFT}} + \Sigma_{kl}^{GW} - \Sigma_{kl}^{\text{dc}}. \quad (18)$$

According to Ref.,<sup>15</sup> the double counting is defined as

$$\Sigma_{kl}^{\text{dc}}(\tau) = - \sum_{mn}^A G_{mn}(\tau) W_{mknl}(\tau) = -f^A G f^A W. \quad (19)$$

The self energy is then given as

$$\begin{aligned} \Sigma_{kl}^{\text{EDMFT}+GW} &= \Sigma_{kl}^{\text{EDMFT}} - \sum_{mn}^{A+E} G_{mn}(\tau) W_{mknl}(\tau) + \sum_{mn}^A G_{mn}(\tau) W_{mknl}(\tau) \\ &= \Sigma_{kl}^{\text{EDMFT}} - \sum_{mn}^E G_{mn}(\tau) W_{mknl}(\tau). \end{aligned} \quad (20)$$

Thus, we find that the double counting corrections adopted in EDMFT+*GW* and QDET are the same if the  $G_0W_0$  approximation is employed for the environment in EDMFT+*GW*. In that case, Eq. 19 becomes identical to Eq. 29 in the main text.

## 5 Implementation details

### 5.1 Implementation of exchange and correlation self-energy

The screened Coulomb potential  $W_0$  is defined in Eq. 19 as  $W_0^{-1} = v^{-1} - P_0$ , where  $P_0$  is the irreducible polarizability. Equivalently, it can be expressed in terms of the reducible polarizability  $\chi = P_0 + P_0 v \chi$  as  $W_0 = v + v \chi v \equiv v + W^{\text{P}}$ .<sup>1</sup> This separation of the screened Coulomb interaction into  $v$  and  $W^{\text{P}}(\omega)$  allows us to separate the exchange-correlation self-energy  $\Sigma_{\text{xc}}$  in Eq. 17 of the main text into the exchange part  $\Sigma_{\text{x}}$  and correlation part  $\Sigma_{\text{c}}$ . The former is given by

$$[\Sigma_{\text{x}}]_{mn} = - \sum_k^{A+E} n_k \langle \psi_m^{\text{KS}} \psi_k^{\text{KS}} | v | \psi_n^{\text{KS}} \psi_k^{\text{KS}} \rangle, \quad (21)$$

where  $\psi^{\text{KS}}$  are the Kohn-Sham eigenstates and  $n_k$  is the occupation number of the state  $\psi_k^{\text{KS}}$ . The correlation contribution  $\Sigma_{\text{c}}$  is determined by evaluating Eq. 17 in the main text with  $W^{\text{P}}$  instead of  $W$ . A compact expression for  $W^{\text{P}}$  is obtained from the spectral decomposition of the dielectric screening using its eigenvectors that we call the projective dielectric eigenpotentials(PDEP).<sup>1,20</sup> The PDEPs form a basis set  $\{|\varphi_i\rangle, i = 1 \cdots N_{\text{PDEP}}\}$ , where  $N_{\text{PDEP}}$  is the number of basis functions, which allows us to write  $W^{\text{P}}$  as

$$W^{\text{P}}(\omega) \approx \Xi^{\text{P}}(\omega) + \sum_{i,j=1}^{N_{\text{PDEP}}} |\tilde{\varphi}_i\rangle \Lambda_{ij}(\omega) \langle \tilde{\varphi}_j|. \quad (22)$$

where  $\Xi^{\text{P}}(\omega) = 4\pi e^2 \int_{R_q=0} \frac{dq}{(2\pi)^3} \frac{\bar{\chi}_{00}}{q^2}$  is the head of  $W^{\text{P}}$ , and  $\bar{\chi}_{00}$  is the head of the symmetrized polarizability  $\bar{\chi} = v^{1/2} \chi v^{1/2}$ . The functions  $|\tilde{\varphi}_i\rangle = v^{\frac{1}{2}} |\varphi_i\rangle$  are the symmetrized PDEP basis functions. The matrix elements  $\Lambda_{ij}$  are elements of the body of  $\bar{\chi}$ . The compact expression for  $W^{\text{P}}$  in the PDEP basis makes it possible to calculate the Green's function and polarizability without explicit summations over unoccupied states through the Lanczos algorithm.<sup>1</sup>

Using contour deformation techniques,  $\Sigma_c$  is decomposed into an integral  $I$  along the imaginary axis and a residue part  $R$ . The former can be further decomposed into three parts:  $I_1$  from the head of  $W_0$ ,  $I_2$  from the body of  $W_0$  with an explicit summation over electronic states, and  $I_3$  from the body of  $W_0$  evaluated by the Lanczos algorithm with  $N_{\text{Lanczos}}$  Lanczos chains. The residue part  $R$  is split into two parts:  $R_1$  from the head of  $W_0$  and  $R_2$  from the body of  $W_0$ . Thus, the correlation part of the self-energy is given by

$$[\Sigma_c]_{mn}(\omega) = [I_1]_{mn}(\omega) + [I_2]_{mn}(\omega) + [I_3]_{mn}(\omega) + [R_1]_{mn}(\omega) + [R_2]_{mn}(\omega), \quad (23)$$

where

$$[I_1]_{mn}(\omega) = \delta_{mn} \int_0^{+\infty} \frac{d\omega'}{\pi} \Xi^P(\omega') \left( \frac{(\epsilon_n^{\text{KS}} - \omega)}{(\epsilon_n^{\text{KS}} - \omega)^2 + \omega'^2} \right) \quad (24)$$

$$[I_2]_{mn}(\omega) = \int_0^{+\infty} \frac{d\omega'}{\Omega\pi} \left( \sum_k^{N_{\text{occ}}+N_{\text{unocc}}} \sum_{i,j=1}^{N_{\text{PDEP}}} \Lambda_{ij}(\omega') \langle \varphi_m^i | \psi_k^{\text{KS}} \rangle \langle \psi_k^{\text{KS}} | \varphi_n^j \rangle \frac{(\epsilon_k^{\text{KS}} - \omega)}{(\epsilon_k^{\text{KS}} - \omega)^2 + \omega'^2} \right) \quad (25)$$

$$[I_3]_{mn}(\omega) = \int_0^{+\infty} \frac{d\omega'}{\Omega\pi} \left( \sum_{i,j=1}^{N_{\text{PDEP}}} \sum_{q_1, q_2=1}^{N_{\text{Lanczos}}} \Lambda_{ij}(\omega') \langle \varphi_m^i | [\xi_n^j]_{q_1} \rangle [U_n^j]_{q_1 q_2} [U_n^j]_{1 q_2} \frac{([\epsilon_n^j]_{q_2} - \omega)}{([\epsilon_n^j]_{q_2} - \omega)^2 + \omega'^2} \right) \quad (26)$$

$$[R_1]_{mn}(\omega) = \sum_k^{N_{\text{occ}}+N_{\text{unocc}}} \delta_{mn} \delta_{nk} f_k \Xi^P(\epsilon_k^{\text{KS}} - \omega) \quad (27)$$

$$[R_2]_{mn}(\omega) = \frac{1}{\Omega} \left( \sum_k^{N_{\text{occ}}+N_{\text{unocc}}} \sum_{i,j=1}^{N_{\text{PDEP}}} \Lambda_{ij}(\omega') \langle \varphi_m^i | \psi_k^{\text{KS}} \rangle f_k \langle \psi_k^{\text{KS}} | \varphi_n^j \rangle \right) \quad (28)$$

$$f_k = \begin{cases} 1 - n_k & \epsilon_{\text{F}'}^{\text{KS}} < \epsilon_k^{\text{KS}} < \omega \\ -n_k & \omega < \epsilon_k^{\text{KS}} < \epsilon_{\text{F}}^{\text{KS}} \\ 0 & \text{otherwise.} \end{cases} \quad (29)$$

Here  $|\xi_n^j\rangle$ ,  $\epsilon_n^j$  and  $U_n^j$  are the Lanczos chain, eigenvalue and unitary matrix for the right vector  $|\varphi_n^j\rangle = |\psi_n^{\text{KS}} \tilde{\varphi}_j^*\rangle$ , respectively, using the Lanczos algorithm as presented in Sec. 2.4 of Ref.

1. The quantities  $\epsilon_F^{\text{KS}}$  and  $\epsilon_{F'}^{\text{KS}}$  are the energies of the highest partially occupied and highest fully occupied KS orbital, respectively,  $\Omega$  is the volume of the cell.

## 5.2 Implementation of double counting contribution to the self-energy

We evaluate  $\Sigma_{\text{xc}}^{\text{dc}}$  and  $\Delta\Sigma_{\text{xc}}$  defined in Eq. 24 and 28 of the main text, respectively, by introducing in Eq. 28 in the main text the following expressions for  $W$  and  $G$ :  $W = v + W^{\text{p}}$ , and  $G_0 = G_0^A + G_0^R$ . This leads to the following definitions

$$\begin{aligned}\Sigma_{\text{xc}}^{\text{dc}}(\omega) &= \Sigma^{\text{x,dc}} + \Sigma^{\text{c,dc}}(\omega) \approx i \int_{-\infty}^{+\infty} \frac{d\omega'}{2\pi} G_0^A(\omega + \omega') v + i \int_{-\infty}^{+\infty} \frac{d\omega'}{2\pi} G_0^A(\omega + \omega') W^{\text{p}}(\omega') \quad (30) \\ \Delta\Sigma_{\text{xc}}(\omega) &= \Delta\Sigma_{\text{x}} + \Delta\Sigma_{\text{c}}(\omega) \approx i \int_{-\infty}^{+\infty} \frac{d\omega'}{2\pi} G_0^R(\omega + \omega') v + i \int_{-\infty}^{+\infty} \frac{d\omega'}{2\pi} G_0^R(\omega + \omega') W^{\text{p}}(\omega').\end{aligned}\quad (31)$$

The active space is formed by  $N_A$  orbitals, while the environment consists of  $N_E$  explicit orbitals and the continuum of unoccupied orbitals. As such,  $N_{\text{occ}} + N_{\text{unocc}} = N_A + N_E$ . Similar derivations to those for  $\Sigma_{\text{xc}}$  (Sec. 5.1) lead to

$$[\Sigma_{\text{x}}^{\text{dc}}]_{mn} = - \sum_k^{N_A} n_k \langle \psi_m^{\text{KS}} \psi_k^{\text{KS}} | v | \psi_n^{\text{KS}} \psi_k^{\text{KS}} \rangle \quad (32)$$

$$[\Sigma_{\text{c}}^{\text{dc}}]_{mn}(\omega) = [I_1]_{mn}(\omega) + [I_2^{\text{dc}}]_{mn}(\omega) + [R_1]_{mn}(\omega) + [R_2^{\text{dc}}]_{mn}(\omega) \quad (33)$$

$$[\Delta\Sigma_{\text{x}}]_{mn} = - \sum_k^{N_E} n_k \langle \psi_m^{\text{KS}} \psi_k^{\text{KS}} | v | \psi_n^{\text{KS}} \psi_k^{\text{KS}} \rangle \quad (34)$$

$$[\Delta\Sigma_{\text{c}}]_{mn}(\omega) = [\Delta I_2]_{mn}(\omega) + [I_3]_{mn}(\omega) + [\Delta R_2]_{mn}(\omega), \quad (35)$$

where

$$[I_2^{\text{dc}}]_{mn}(\omega) = \int_0^{+\infty} \frac{d\omega'}{\Omega\pi} \left( \sum_k^{N_A} \sum_{i,j=1}^{N_{\text{PDEP}}} \Lambda_{ij}(\omega') \langle \varphi_m^i | \psi_k^{\text{KS}} \rangle \langle \psi_k^{\text{KS}} | \varphi_n^j \rangle \frac{(\epsilon_k^{\text{KS}} - \omega)}{(\epsilon_k^{\text{KS}} - \omega)^2 + \omega'^2} \right) \quad (36)$$

$$[R_2^{\text{dc}}]_{mn}(\omega) = \frac{1}{\Omega} \left( \sum_k^{N_A} \sum_{i,j=1}^{N_{\text{PDEP}}} \Lambda_{ij}(\omega') f_k \langle \varphi_m^i | \psi_k^{\text{KS}} \rangle \langle \psi_k^{\text{KS}} | \varphi_n^j \rangle \right) \quad (37)$$

$$[\Delta I_2]_{mn}(\omega) = \int_0^{+\infty} \frac{d\omega'}{\Omega\pi} \left( \sum_k^{N_E} \sum_{i,j=1}^{N_{\text{PDEP}}} \Lambda_{ij}(\omega') \langle \varphi_m^i | \psi_k^{\text{KS}} \rangle \langle \psi_k^{\text{KS}} | \varphi_n^j \rangle \frac{(\epsilon_k^{\text{KS}} - \omega)}{(\epsilon_k^{\text{KS}} - \omega)^2 + \omega'^2} \right) \quad (38)$$

$$[\Delta R_2]_{mn}(\omega) = \frac{1}{\Omega} \left( \sum_k^{N_E} \sum_{i,j=1}^{N_{\text{PDEP}}} \Lambda_{ij}(\omega') f_k \langle \varphi_m^i | \psi_k^{\text{KS}} \rangle \langle \psi_k^{\text{KS}} | \varphi_n^j \rangle \right). \quad (39)$$

## 6 Convergence of QDET calculations

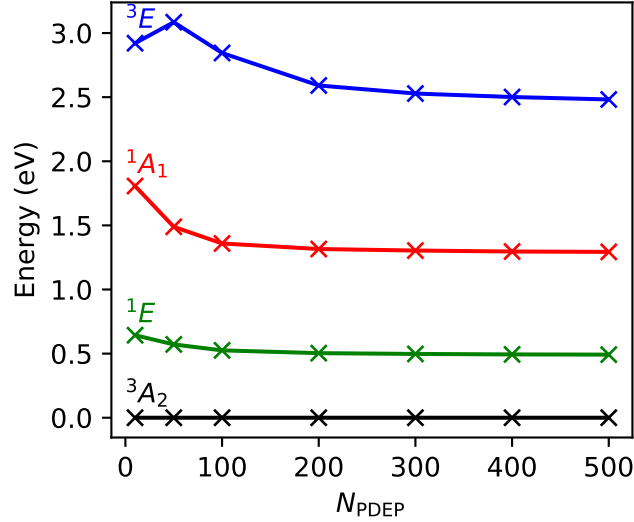


Figure S1: Computed vertical excitation energies of the  $\text{NV}^-$  center in diamond as a function of the number of eigenpotentials  $N_{\text{PDEP}}$ . Calculations are performed in a 511-atom cell using the PBE functional.

### 6.1 Number of dielectric eigenpotentials

In Fig. S1 we show the convergence of the vertical excitation energies for  $\text{NV}^-$  in a 511-atom cell using PBE with respect to the number of PDEP eigenpotentials,  $N_{\text{PDEP}}$ . A 6-orbital model (see Sec. 4 of the main text) is adopted. The plot shows that 500 PDEP eigenpotentials yield converged excitation energies within 0.02 eV.

### 6.2 Composition of the active space

As shown in Fig. (6) of the main text, localized defect orbitals of the  $\text{SiV}^0$  defect in diamond are found in the valence band, the band gap, and the conduction band of the host material. Ideally, all localized orbitals should be included in the active space. However, the computational complexity of full configuration interaction (FCI) grows exponentially when increasing the number of occupied and unoccupied orbitals simultaneously, making a

straightforward convergence relative to all localized orbitals impractical. To reduce the computational cost, we do not include in the active space those localized orbitals with energies above the conduction band minimum (CBM)) in all calculations in the main text. To verify that excluding those localized orbitals from the active space does not influence the results, we compare excitation energies obtained with the minimal model<sup>21</sup> with those of a model including the most localized orbital within the conduction band. We find that the excitation energies change by less than 0.05 eV. Hence, in all calculations presented in the main text we only considered the defect orbitals within the valence band, in addition to those in the minimal model.



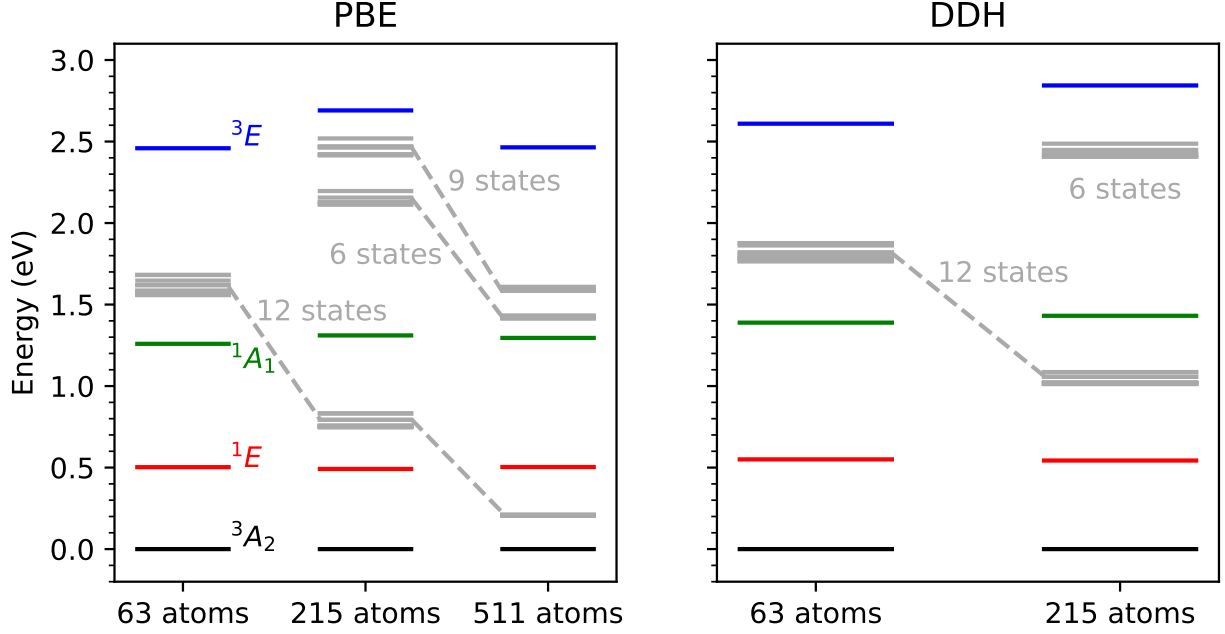


Figure S2: Computed excitation energies (eV) for the  $\text{NV}^-$  center in diamond obtained from calculations with the PBE (left) and DDH functional (right). Ghost states (see text) are shown in grey. We find 12 nearly-degenerate single excitations from the  $e$  states to the conduction band, 6 single excitations from the  $a_1$  state to the conduction band, and 9 double excitations from the  $e$  state to the conduction band. The convergence of the ghost states is indicated with the dotted lines.

## 7 Ghost states

We find that in QDET, unphysical excitations occur in some cases when conduction and valence orbitals are included in the active space. These unphysical excitations, which we denote as *ghost states*, correspond to excitations from the defect to the conduction band, but with excitation energies that are unphysically low. Below, for the example of the  $\text{NV}^-$  defect in diamond, we analyze the origin of these ghost states. We note that our detailed analysis reveals that ghost states occur with HFDC as well, and we will discuss those for the example of the  $\text{SiV}^0$  defect in diamond.

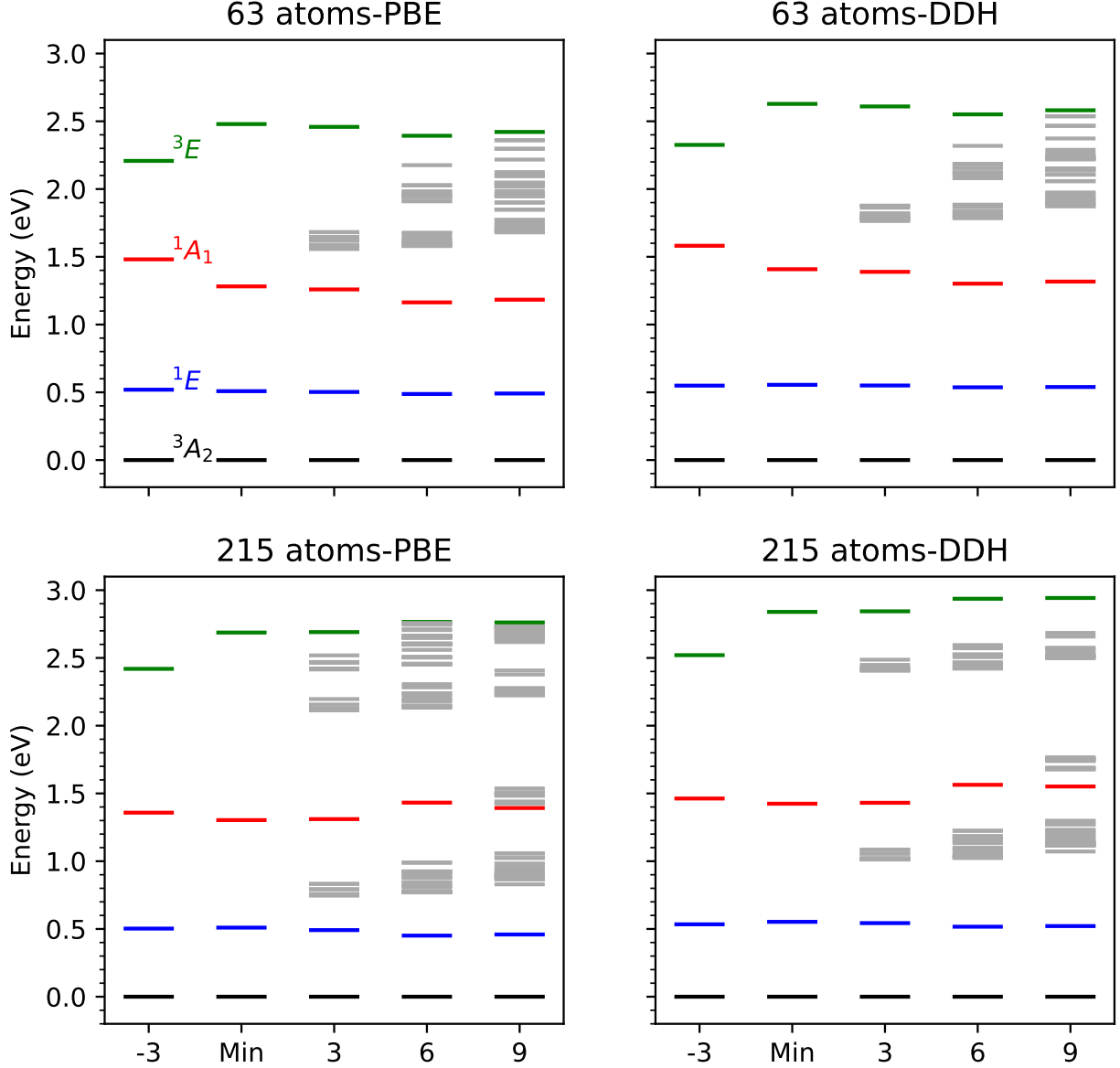


Figure S3: Excitation energies (eV) of the  $\text{NV}^-$  in diamond as a function of the active space size for a 63- (top) and 215-atom supercell (bottom). Calculations are performed with the PBE (left) and DDH functional (right). “Min” denotes the minimal model, “-3” indicates that three additional valance band orbitals are added to the minimal model, “3” indicates that three additional conduction band orbitals are added to the minimal model, and so forth.

## 7.1 $\text{NV}^-$ in diamond

Using  $\text{NV}^-$  as an example, we investigate the origin of ghost states. For the 63-atom and 215-atom supercells, we adopt a minimum model, *i.e.* we include in the active space the two defect  $e$  and two defect  $a_1$  orbitals,<sup>2</sup> and the three lowest conduction band orbitals. For

the 511-atom cell we adopt a model which includes 6 orbitals, as mentioned in Sec. 4 of the main text, and the three lowest conduction orbitals.

In Fig. S2 and S3, we show both the defect excitations and the ghost states as a function of the supercell size and the active-space size, respectively. The energy of the ghost states decreases with increasing supercell size but gradually increases with increasing size of the active space. Considering that QDET is exact in the limit of an infinitely large supercell and an infinitely large active space, the results suggest that the slow convergence w.r.t. the active space size is the reason for the existence of ghost states. Furthermore, we speculate that this problem may be material dependent. As the slow convergence only affects the transitions to the conduction-band orbitals, and not those within the defect, it is reasonable to expect that the slow convergence originates from an inadequate description of conduction-band orbitals when the Brillouin zone is only sampled at the  $\Gamma$ -point. Diamond is an indirect bandgap semiconductor, and its conduction band minimum requires an accurate  $\mathbf{k}$ -point sampling.

## 7.2 $V_S^0$ in ZnS

In order to test our hypothesis, we study the neutral sulphur vacancy in cubic ZnS ( $V_S^0$ ). As a direct bandgap material, cubic ZnS has a three-fold degenerate valence-band minimum (VBM) and a non-degenerate conduction-band minimum (CBM). Again, we use the localization factor defined in Eq. 30 of the main text and shown in Fig. S4 to determine the orbitals to include in the active space. We find that a neutral sulphur vacancy introduces four defect orbitals originating from the four dangling bonds of Zn, one of which is slightly lower than the VBM and a three-fold degenerate one slightly above the CBM. We include the VBM and CBM in the active space to form an eight-orbital active space.

In Fig. S5 we show the vertical excitation energies of  $V_S^0$  as functions of supercell size. Similar to  $NV^-$ , the excitation energies within the defect are relatively stable when increasing the supercell size. In contrast to  $NV^-$ , both the excitation energies from the defect to the CBM and those from the VBM to the CBM are also stable when increasing the supercell

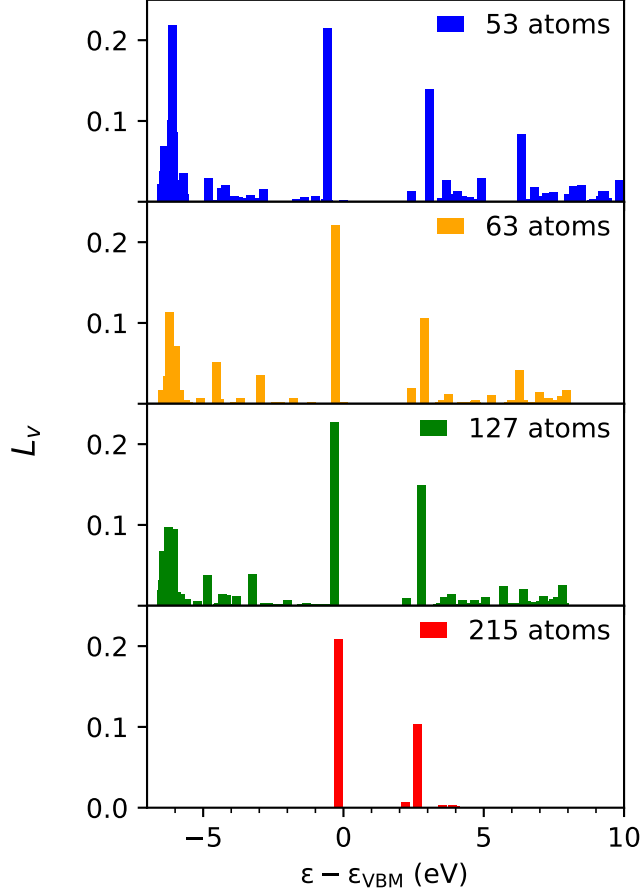


Figure S4: Localization factor ( $L_V$ , see Eq. 30 in the main text) for the  $V_S^0$  in ZnS as a function of the Kohn-Sham energy relative to the VBM. Results are shown for 4 different supercell sizes.

size. This confirms our hypothesis that the unphysical excitations found in diamond are due to an inaccurate description of the CBM due to the indirect bandgap of the system.

In summary, we find excitations with unphysically low energies occurring in QDET calculations for materials with indirect bandgaps for supercells for which the  $\Gamma$ -point sampling is insufficient to correctly sample the CBM. Our analysis shows that the photoionization energies (excitation energies to the CBM) increase with increasing active space size, but the convergence is slow. We find that these energies are due to an inaccurate sampling of the CBM of an indirect-bandgap material in the supercells used here. This finding is confirmed by our investigation of the photoionization in the  $V_S^0$  in the direct-bandgap insulator ZnS,

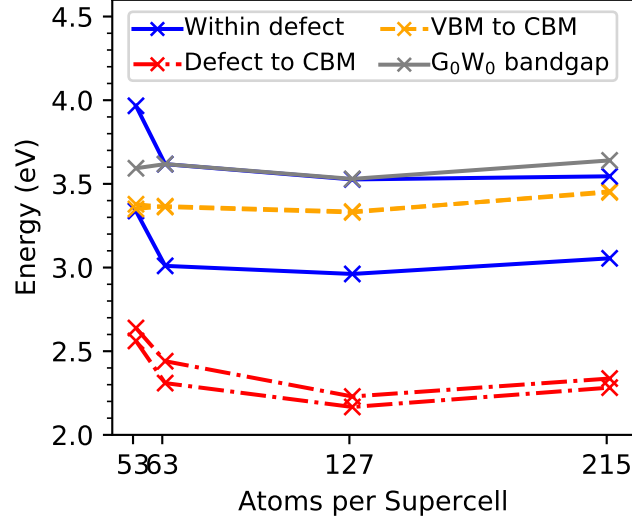


Figure S5: Vertical excitation energies (eV) of the  $V_S^0$  defect in ZnS as functions of supercell size.

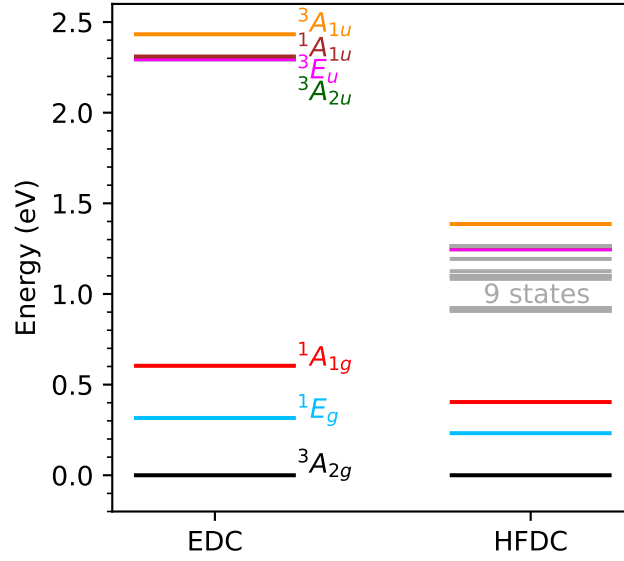


Figure S6: Vertical excitation energies for the  $SiV_0$  center in diamond in a 215-atom cell. Calculations are performed with the EDC (left) and HFDC (right) correction schemes (see text). The 9 ghost states in the calculations with HFDC are shown in grey. These ghost states represent excitations from the valence band to the defect orbitals.

where we do not observe any ghost states.

### 7.3 SiV<sup>0</sup> in diamond

Our analysis of ghost states in diamond reveals that ghost states occur in QDET calculations using HFDC. In Fig. S6 we present a detailed comparison between the vertical excitation spectrum obtained when using the two double counting schemes for SiV<sup>0</sup> in a 215-atom cell, using the same computational setup as that of Ref. 2. Notably, HFDC introduces 9 *ghost states*, which correspond to excitations from the valance band to the defect orbitals but have lower excitation energies than those within the defect. We note that these *ghost states* do not occur in calculations with the EDC scheme. As the VBM of diamond is found at the  $\Gamma$ -point in reciprocal space, these ghost states do not originate from the bandstructure folding, but rather from the incomplete double counting correction within HF. As the approximate HFDC scheme affects localized defect orbitals differently than delocalized valence orbitals, excitations with unphysical energies occur.

## 8 Vertical excitation energies

Table S1: Vertical excitation energies (eV) of  $\text{NV}^-$ ,  $\text{SiV}^0$ ,  $\text{GeV}^0$ ,  $\text{SnV}^0$  and  $\text{PbV}^0$  in diamond. All calculations use the PBE functional. Experimental measurements of zero phonon line (ZPL) energies are shown in brackets in the last column. Reference vertical excitation energies are computed from experimental ZPL when Stokes energies are available. Results are shown for calculations with the exact double counting (EDC) and Hartree-Fock double counting (HFDC) schemes (see text). Energy levels are labelled using the representations of the  $C_{3v}$  point group.

| System           | Excitation                   | EDC        |       |       | HFDC       |       |       | Ref  |
|------------------|------------------------------|------------|-------|-------|------------|-------|-------|--|
|                  |                              | # of atoms |       |       | # of atoms |       |       |  |
|                  |                              | 63         | 215   | 511   | 63         | 215   | 511   |  |
| NV <sup>-</sup>  | <sup>1</sup> E               | 0.512      | 0.459 | 0.463 | 0.419      | 0.380 | 0.375 | 2.180 <sup>22</sup> (1.945 <sup>22</sup> ) |
|                  | <sup>1</sup> A <sub>1</sub>  | 1.526      | 1.305 | 1.270 | 1.253      | 1.174 | 1.150 |  |
|                  | <sup>3</sup> E               | 1.944      | 2.023 | 2.152 | 1.516      | 1.381 | 1.324 |  |
| SiV <sup>0</sup> | <sup>1</sup> E <sub>g</sub>  | 0.309      | 0.324 | 0.321 | 0.184      | 0.209 | 0.236 | (1.31 <sup>23</sup> )                      |
|                  | <sup>1</sup> A <sub>1g</sub> | 0.604      | 0.645 | 0.642 | 0.326      | 0.380 | 0.435 |  |
|                  | <sup>3</sup> A <sub>2u</sub> | 2.295      | 2.003 | 2.146 | 1.710      | 1.223 | 1.098 |  |
|                  | <sup>3</sup> E <sub>u</sub>  | 2.319      | 2.011 | 2.161 | 1.744      | 1.229 | 1.096 |  |
|                  | <sup>1</sup> A <sub>1u</sub> | 2.365      | 2.040 | 2.183 | 1.798      | 1.251 | 1.111 |  |
|                  | <sup>3</sup> A <sub>1u</sub> | 2.541      | 2.183 | 2.260 | 1.952      | 1.382 | 1.188 |  |
| GeV <sup>0</sup> | <sup>1</sup> E <sub>g</sub>  | 0.363      | 0.334 | 0.357 | 0.243      | 0.260 | 0.289 |  |
|                  | <sup>1</sup> A <sub>1g</sub> | 0.721      | 0.671 | 0.717 | 0.451      | 0.496 | 0.554 |  |
|                  | <sup>3</sup> A <sub>2u</sub> | 3.062      | 2.661 | 2.924 | 2.098      | 1.579 | 1.456 |  |
|                  | <sup>3</sup> E <sub>u</sub>  | 3.069      | 2.653 | 2.925 | 2.117      | 1.573 | 1.443 |  |
|                  | <sup>1</sup> A <sub>1u</sub> | 3.089      | 2.661 | 2.940 | 2.151      | 1.581 | 1.443 |  |
|                  | <sup>3</sup> A <sub>1u</sub> | 3.235      | 2.756 | 2.970 | 2.281      | 1.676 | 1.495 |  |
| SnV <sup>0</sup> | <sup>1</sup> E <sub>g</sub>  | 0.353      | 0.341 | 0.295 | 0.266      | 0.277 | 0.276 |  |
|                  | <sup>1</sup> A <sub>1g</sub> | 0.711      | 0.686 | 0.596 | 0.510      | 0.538 | 0.551 |  |
|                  | <sup>3</sup> A <sub>2u</sub> | 3.050      | 2.722 | 2.590 | 2.126      | 1.573 | 1.459 |  |
|                  | <sup>3</sup> E <sub>u</sub>  | 3.058      | 2.707 | 2.571 | 2.142      | 1.561 | 1.444 |  |
|                  | <sup>1</sup> A <sub>1u</sub> | 3.079      | 2.701 | 2.561 | 2.172      | 1.558 | 1.436 |  |
|                  | <sup>3</sup> A <sub>1u</sub> | 3.192      | 2.796 | 2.616 | 2.281      | 1.654 | 1.491 |  |
| PbV <sup>0</sup> | <sup>1</sup> E <sub>g</sub>  | 0.379      | 0.352 | 0.319 | 0.293      | 0.300 | 0.302 |  |
|                  | <sup>1</sup> A <sub>1g</sub> | 0.751      | 0.704 | 0.640 | 0.563      | 0.587 | 0.600 |  |
|                  | <sup>3</sup> A <sub>2u</sub> | 3.604      | 3.227 | 3.095 | 2.482      | 1.905 | 1.788 |  |
|                  | <sup>3</sup> E <sub>u</sub>  | 3.609      | 3.206 | 3.072 | 2.496      | 1.888 | 1.768 |  |
|                  | <sup>1</sup> A <sub>1u</sub> | 3.623      | 3.193 | 3.056 | 2.520      | 1.879 | 1.755 |  |
|                  | <sup>3</sup> A <sub>1u</sub> | 3.719      | 3.275 | 3.099 | 2.606      | 1.963 | 1.796 |  |

## References

- (1) Govoni, M.; Galli, G. Large Scale GW Calculations. *J. Chem. Theory. Comput.* **2015**, *11*, 2680–2696.
- (2) Ma, H.; Sheng, N.; Govoni, M.; Galli, G. First-Principles Studies of Strongly Correlated States in Defect Spin Qubits in Diamond. *Phys. Chem. Chem. Phys.* **2020**, *22*, 25522–25527.
- (3) Ma, H.; Govoni, M.; Galli, G. Quantum Simulations of Materials on Near-Term Quantum Computers. *npj Comput. Mater.* **2020**, *6*, 1–8.
- (4) Ma, H.; Sheng, N.; Govoni, M.; Galli, G. Quantum Embedding Theory for Strongly Correlated States in Materials. *J. Chem. Theory. Comput.* **2021**, *17*, 2116–2125.
- (5) Muechler, L.; Badrtdinov, D. I.; Hampel, A.; Cano, J.; Rösner, M.; Dreyer, C. E. Quantum embedding methods for correlated excited states of point defects: Case studies and challenges. *arXiv:2105.08705 [cond-mat]* **2021**, arXiv: 2105.08705.
- (6) Georges, A.; Kotliar, G. Hubbard Model in Infinite Dimensions. *Phys. Rev. B* **1992**, *45*, 6479–6483.
- (7) Georges, A.; Kotliar, G.; Krauth, W.; Rozenberg, M. J. Dynamical Mean-Field Theory of Strongly Correlated Fermion Systems and the Limit of Infinite Dimensions. *Rev. Mod. Phys.* **1996**, *68*, 13–125.
- (8) Georges, A. Strongly Correlated Electron Materials: Dynamical Mean-Field Theory and Electronic Structure. *AIP Conf. Proc.* **2004**, *715*, 3–74.
- (9) Anisimov, V. I.; Poteryaev, A. I.; Korotin, M. A.; Anokhin, A. O.; Kotliar, G. First-Principles Calculations of the Electronic Structure and Spectra of Strongly Correlated Systems: Dynamical Mean-Field Theory. *J. Phys. Condens. Matter.* **1997**, *9*, 7359–7367.



- (10) Kotliar, G.; Savrasov, S. Y.; Haule, K.; Oudovenko, V. S.; Parcollet, O.; Marianetti, C. A. Electronic Structure Calculations with Dynamical Mean-Field Theory. *Rev. Mod. Phys.* **2006**, *78*, 865–951.
- (11) Biermann, S.; Aryasetiawan, F.; Georges, A. First-Principles Approach to the Electronic Structure of Strongly Correlated Systems: Combining the GW Approximation and Dynamical Mean-Field Theory. *Phys. Rev. Lett.* **2003**, *90*, 086402.
- (12) Biermann, S. Dynamical Screening Effects in Correlated Electron Materials—a Progress Report on Combined Many-Body Perturbation and Dynamical Mean Field Theory: ‘GW+DMFT’. *J. Phys. Condens. Matter.* **2014**, *26*, 173202.
- (13) Boehnke, L.; Nilsson, F.; Aryasetiawan, F.; Werner, P. When Strong Correlations Become Weak: Consistent Merging of GW and DMFT. *Phys. Rev. B* **2016**, *94*, 201106.
- (14) Choi, S.; Kutepov, A.; Haule, K.; van Schilfgaarde, M.; Kotliar, G. First-Principles Treatment of Mott Insulators: Linearized QSGW+DMFT Approach. *npj Quantum Mater.* **2016**, *1*, 1–6.
- (15) Nilsson, F.; Boehnke, L.; Werner, P.; Aryasetiawan, F. Multitier Self-Consistent GW+EDMFT. *Phys. Rev. Materials* **2017**, *1*, 043803.
- (16) Sun, P.; Kotliar, G. Extended Dynamical Mean-Field Theory and GW Method. *Phys. Rev. B* **2002**, *66*, 085120.
- (17) Tomczak, J. M.; Casula, M.; Miyake, T.; Aryasetiawan, F.; Biermann, S. Combined GW and Dynamical Mean-Field Theory: Dynamical Screening Effects in Transition Metal Oxides. *Europhys. Lett.* **2012**, *100*, 67001.
- (18) Lee, J.; Haule, K. Diatomic Molecule as a Testbed for Combining DMFT with Electronic Structure Methods Such as GW and DFT. *Phys. Rev. B* **2017**, *95*, 155104.

- (19) Smith, J. L.; Si, Q. Spatial Correlations in Dynamical Mean-Field Theory. *Phys. Rev. B* **2000**, *61*, 5184–5193.
- (20) Wilson, H. F.; Gygi, F.; Galli, G. Efficient iterative method for calculations of dielectric matrices. *Phys. Rev. B* **2008**, *78*, 113303.
- (21) Thiering, G.; Gali, A. The  $(eg \otimes eu) \otimes Eg$  product Jahn–Teller effect in the neutral group-IV vacancy quantum bits in diamond. *npj Comput. Mater.* **2019**, *5*, 18.
- (22) Davies, G.; Hamer, M. F.; Price, W. C. Optical Studies of the 1.945 eV Vibronic Band in Diamond. *Proc. R. Soc. London A* **1976**, *348*, 285–298.
- (23) Green, B. L.; Doherty, M. W.; Nako, E.; Manson, N. B.; D’Haenens-Johansson, U. F. S.; Williams, S. D.; Twitchen, D. J.; Newton, M. E. Electronic Structure of the Neutral Silicon-Vacancy Center in Diamond. *Phys. Rev. B* **2019**, *99*, 161112.